ACS OMEGA

http://pubs.acs.org/journal/acsodf

Article

Engineering the Morphostructural Properties and Drug Loading Degree of Organic–Inorganic Fluorouracil–MgAl LDH Nanohybrids by Rational Control of Hydrothermal Treatment

Alina Ibanescu, Dragos-Ioan Olariu, Doina Lutic, Vasile Hulea, and Brindusa Dragoi*

Cite This: *ACS Omega* 2023, 8, 26102–26121

Read Online

ACCESS | Metrics & More | Article Recommendations | Supporting Information

ABSTRACT: Layered double hydroxides (LDHs) or hydrotalcite-like compounds have attracted great attention for the delivery of anticancer drugs due to their 2D structure, exhibiting a high surface-to-volume ratio and a high chemical versatility. The drug is protected between the layers from which it is slowly released, thus increasing the therapeutic effect and minimizing the side effects associated to nonspecific targeting. This work aimed to design LDHs with Mg and Al (molar ratio of 2/1) in brucite-like layers, which retained fluorouracil (5-FU; 5-FU/Al = 1, molar ratio) in the interlayer gallery as the layers grow during the co-precipitation step of the synthesis. To rationally control the physicochemical properties, particularly the size of the crystallites, the aging step following the co-precipitation was performed under carefully controlled conditions by changing the time and temperature (i.e., 25 °C for 16 h, 100 °C for 16 h, and 120 °C for 24 h). The results revealed the achievement of the control of the size of the crystals, which are gathered in three different agglomeration systems, from tight to loose, as well as the loading degree of the drug in the final organic–inorganic hybrid nanomaterials. The role played by the factors and parameters affecting the drug-controlled release was highlighted by assessing the release behavior of 5-FU by changing the pH, solid mass/volume ratio, and ionic strength. The results showed a pH-dependent behavior but not necessarily in a direct proportionality. After a certain limit, the mass of the solid diminishes the rate of release, whereas the ionic strength is essential for the payload discharge.

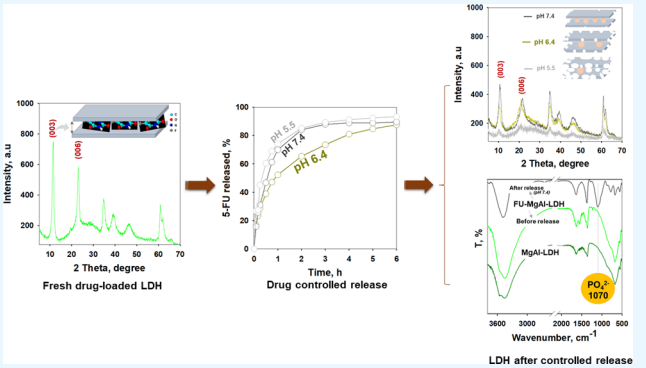

1. INTRODUCTION

Chemotherapy is the main strategy in the fight against cancer, especially for patients who are not eligible for local treatments, such as surgery and/or radiotherapy.[1] However, the therapeutic effect is often limited by the resistance mechanisms developed by the host against the drug, while the treatment itself is accompanied by side effects due to the systemic exposure. In addition, certain drugs can be chemically changed upon contact with body fluids or are incapable to cross the biological barriers, both situations considerably decreasing the on-target therapeutic effect. All these factors make cancer the second leading cause of death after heart attacks.[2] 5-Fluorouracil (5-FU) is one of the currently used drugs against various types of cancer, such as colorectal cancer, breast cancer, pancreatic cancer, and stomach cancer. Because of its intravenous administration, FU is distributed in the entire body and not only to the ill cells, causing severe toxic effects. Moreover, the developed drug resistance to this drug is generally acknowledged.[3,4] To overcome these unwanted side effects and maximize the therapeutic effect while decreasing the administrated dose, new formulations of the drug are necessary. The progress made in nanoscience and nanotechnology offers new options for drug formulations, that is, nanoformulations. Essentially, the organic molecule acting as drug is encapsulated in a nanometric carrier (nanoparticle, NP), which has the potential to properly address most of the issues raised by these simple drug molecules. Hence, the encapsulation of drug molecules into NPs can significantly improve their pharmacokinetics, biocompatibility, and biodistribution.[5] Still, the physicochemical properties associated with the nanometric scale and nonbiologic source make the application of NPs a slower process than expected. This delay is however quite normal because the complexity of the nanodrugs (NDs) in comparison with the much simpler organic molecules requires a more extensive and in-depth characterization of the properties aiming at providing the most appropriate nanodrugs in terms of efficacy and safety. In

Received: April 5, 2023
Accepted: June 13, 2023
Published: July 12, 2023

addition, if NPs are inorganic, the design and characterization require more efforts to finally provide the right ND for the right tumor. Another factor considered in the design of NDs is the administration route. For instance, intravenous administration of NDs, which is the most complex route, involves four key stages from the administration point to the tumor, as follows: (i) transport and circulation in a complex vascular network with red blood cells, white blood cells, and many others; (ii) margination from the central stream of the blood flow to the vessel wall region and firm adhesion to the endothelium near the tumor site; (iii) diffusion into tumor tissues through leaky vasculatures, recognition and (iv) internalization by tumor cells.[5] However, to make this journey successfully and then to release the payload into the tumor cells, the ND should exhibit specific physicochemical properties, which can be rationally controlled at the synthesis stage. Of course, NPs are not "magic bullets", but considering the advantages and pitfalls, the obtained results so far encourage the research on this exciting and promising topic.

Among the inorganic NPs used for drug delivery, layered double hydroxides (LDHs) have attracted attention due to their many advantages, such as high biocompatibility, nontoxicity, and adjustable controlled release property.[6] In addition, the plate-like shape of the LDH nanocrystals includes them in the class of nanoparticles with a high aspect ratio, which is more suitable for the prolonged circulation in the bloodstream.[7,8] LDHs have the following chemical formula, $[M^{2+}_{1-x}M^{3+}_{x}(OH)_2]^{x+}(A^{n-})_{x/n}\cdot mH_2O$, which shows the presence of bi- and trivalent cations with similar radii in their composition.[9] Each cation is surrounded by six HO groups forming an octahedron. The octahedra share edges to form theoretically infinite sheets ∼0.48 nm thick, which are on top of each other. The space between the sheets is occupied by anions and water. The anions can cover a large variety of inorganic, organic, and biological species and have the main role of compensating the positive charge brought by the trivalent cations and thus stabilizing the structure. Therefore, this high chemical versatility of LDHs allows the design of a huge family of ND with similar morphostructural properties. The huge amount of work performed so far on LDHs in medical and pharmaceutical fields demonstrates the feasibility of LDHs to function as smart carriers for loading, safe transport, and controlled release of drugs and genes if we limit their application to these types of bioactive molecules only. This interesting topic of LDH-based nanohybrids for medical applications is accurately covered by numerous reviews, and all interested readers are kindly invited to consult and to use them as a starting point to explore these exciting nanomaterials for medicine.[10−14]

Although several works have been reported so far on 5-FU-loaded MgAl-LDH, the research on this system is not yet completed, while the goal of transferring 5-FU-LDH ND to the market requires further work to be achieved. Mainly, the investigations envisage the physicochemical properties of the final ND. Among them, the size and amount of the carried drug are two of the critical parameters to be optimized. The first one controls the fate of the ND in the bloodstream, whereas the amount of drug that can be loaded and the rate of its release govern the frequency of administration.

In this work, we mainly focused on (i) the relationship between the crystallinity and crystal size of the MgAl-LDH (Mg/Al = 2) and the amount of FU incorporated in the final ND, as well as (ii) the evolution of the structural properties of the carriers during the controlled release and the mechanism governing the drug release in relation to the structural properties. To reach this aims, two series of samples were synthesized by co-precipitation at low suprasaturation and constant pH, that is, purely inorganic LDHs and FU-chemically modified LDHs. The rational control of the crystallite size and loading degree in the drug was achieved by changing the experimental conditions during the aging step in a hydrothermal environment following the co-precipitation of cations. Particular attention was given to the temperature and time of the hydrothermal treatment. The experimental results obviously indicated that controlling the experimental conditions during the synthesis is critical to rationally tune the physicochemical properties of the final ND.

2. EXPERIMENTAL SECTION

2.1. Chemicals and Materials. Chemicals used for the synthesis of the different samples synthesized herein are anhydrous $AlCl_3$ (Sigma-Aldrich, 98%) and $MgCl_2$ (Alfa Aesar, 99%) as metal precursors, NaOH (VWR Chemicals, 99.1%) as precipitating agent, 5-FU (Sigma, >99%) as a model anticancer drug, phosphate buffer (Na_2HPO_4 Sigma-Aldrich >99%; NaH_2PO_4 Honeywell >99%), distillated water (Thermo Scientific), EtOH (Honeywell, 99.8%), NaCl (Lachner, 99.97%), KCl (Lachner, 100%), $MgCl_2{\cdot}6H_2O$ (Roth, 99%), and $CaCl_2$ (Lachner, 96.3%).

2.2. Synthesis of LDH. LDHs with M^{2+}/M^{3+} = 2 were synthesized by co-precipitation under low suprasaturation conditions in a double-jacketed reactor from Syrris (UK) connected to a peristaltic pump system (Atlas Syringe Pump), which allows very strict and reproducible control of the solution flow, temperature, pH, and speed of stirring. All these parameters were controlled by the ATLAS software installed on a computer to which the reactor is connected. To synthesize the LDHs, two solutions were prepared. Solution A was prepared by dissolving 2.56 g of $MgCl_2$ (0.0269 mol) and 1.82 g of $AlCl_3$ (0.0136 mol) in distilled water in a 50 mL volumetric flask. Solution B was aqueous 1 M NaOH and employed as the precipitating agent. After preparing the solutions, they were ultrasonicated and filtered to remove any possible solid impurities. This step was also necessary to avoid an unlikely clogging of the tubing through which the pumps introduce the two solutions into the reactor. To start the synthesis, two sensors, a pH meter and a temperature reading sensor, were inserted into the reactor. Temperature control was achieved with the help of a high-precision thermostatic system (Huber, Germany) using silicone oil as a heating agent. A computer equipped with a dedicated interface and software was connected to the entire system, allowing the measurement and storage of working parameters in real time and the digitized control of all components in the system. Before starting the synthesis, 50 mL of water was added to the reactor. Afterward, solutions A and B were introduced simultaneously, with the help of pumps, as follows: at a constant flow rate of 0.5 mL/min (solution A) and variable flow rate (solution B) aiming to preserve the reaction medium at a constant pH of 10 (±0.4). The addition of the two solutions was performed under constant stirring at 250 rpm and 25 °C. Once the co-precipitation of cations was finished, the suspension was transferred into a Teflon autoclave for the hydrothermal treatment (HT). Three different HT conditions were used, as follows: 25 °C for 16 h, 100 °C for 16 h, and 120 °C for 24 h. At the end of the HT, the autoclave was cooled at room

https://doi.org/10.1021/acsomega.3c02288
ACS Omega 2023, 8, 26102−26121

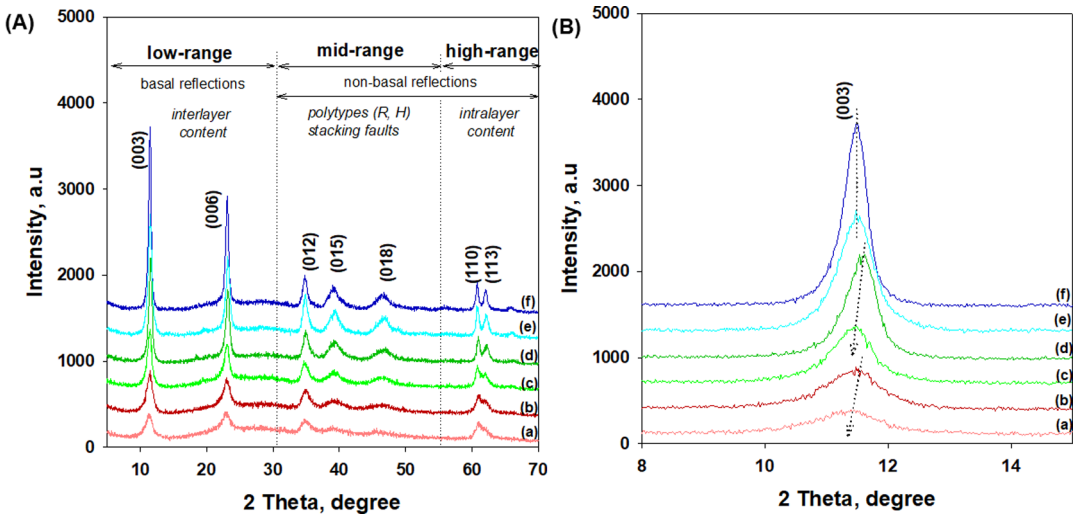

Figure 1. (A) XRD patterns of LDH and 5-FU-LDH aged at different hydrothermal treatments (25 and 100 °C, 16 h; 120 °C, 24 h) after co-precipitation and (B) (003) diffraction peak of samples ((a) 5-FU-LDH-25, (b) LDH-25, (c) 5-FU-LDH-100, (d) LDH-100, (e) 5-FU-LDH-120, and (f) LDH-120)).

temperature. Then, the solids were filtrated and washed with 1 L distilled water to remove residual sodium. The obtained solids were dried at 60 °C overnight. The samples were denoted as LDH_*X*, where *X* is the HT temperature. For the organic−inorganic nanohybrids containing 5-FU, the synthesis was performed under the same conditions as for the bare LDHs except for the addition of the corresponding amount of 5-FU (Al^{3+}/5-FU = 1) in the reaction medium. The samples were labeled as 5-FU_LDH_*X*, where *X* is the HT temperature.

2.3. Physicochemical Characterization of Samples. The chemical composition (Mg, Al) of the samples was determined via absorption atomic spectroscopy (AAS) on a ContrAA 300 apparatus from Analytik Jena after the complete dissolution of samples in concentrated HCl.

The FU-containing samples used for AAS were further employed to calculate the loading capacity (LC, %) and encapsulation efficiency (EE, %). LC is defined as the amount of drug encapsulated in the nanocarrier related to the total amount of drug-containing nanocarrier multiplied by 100. EE is defined as the amount of drug encapsulated in the nanocarrier related to the total amount of drug used for the synthesis multiplied by 100. The amount of 5-FU in the solution was assessed based on absorbance at λ = 266 nm on a Rayleigh UV1800 V/VIS spectrophotometer, and the calculations were done employing the equations below:

$$\text{LC, \%} = \frac{m_{\text{FU in the carrier}}}{m_{\text{carrier}}} \times 100$$

$$\text{EE, \%} = \frac{m_{\text{FU in the carrier}}}{m_{\text{FU total}}} \times 100$$

The amount of drug was evaluated based on a calibration curve constructed for a sequence of 5-FU standard concentrations (0.5−30 μg mL^{-1}). The curve was obtained by plotting the absorbance *vs* the 5-FU concentration (R^2 = 0.9999).

XRD measurements were performed on a Bruker AXS D8 apparatus with monochromatic Cu Kα radiation (λ = 0.15406 nm wavelength) at room temperature. The patterns were recorded from 5 to 70° 2θ, with a step of 0.02°. The crystallite sizes were calculated using the Scherrer equation, $D = \lambda/(\beta \times \cos\theta)$, where λ = the incident ray wavelength (0.15406 nm), β = the peak width at half height (rad) after Warren's correction for instrumental broadening, and θ = the Bragg angle.

Nitrogen physisorption was carried out on a Nova 2200 instrument from Quantachrome. The degassed samples (25 °C, 16 h) were subjected to nitrogen adsorption at −196 °C until the isotherms were completed. The values of textural properties, *i.e.*, surface area and pore volume, were calculated from the corresponding isotherms using the BET equation applied to the 0.09−0.32 relative pressure range and the total pore volume at p/p_0 ∼0.975, respectively.

FTIR spectra of samples diluted in KBr (1 wt %) were collected on a Scimitar FTS 2000 (Digilab) between 400 and 4000 cm^{-1}, 50 acquisitions per spectrum, and a resolution of 4 cm^{-1}.

Scanning electron microscopy (SEM) was performed on a Hitachi S-4800 operated at 5 kV.

Diffuse light scattering (DLS) and zeta potential measurements were performed on an Amerigo Particle Size & Zeta Potential Analyzer from Cordouan Technologies. The particle size was measured using the Vasco-Kin contactless remote optical head, whereas the electrophoretic mobility (μ_e) was measured inside using a dip cell with carbon electrode. The electrode was inserted into the diluted sample (three drops in distilled water) carefully to avoid the formation of gas bubbles. The values of Zeta-average (nm) were calculated by the cumulant analysis method of the autocorrelation function from the Amerigo software.

Thermogravimetric analysis (TG) was performed on a NETZSCH TG 209C apparatus instrument using 20 mg of the sample. The sample was subjected to temperature increase from 50 to 900 °C with a rate of 10 °C min^{-1} under synthetic air (20 mL, min^{-1}).

2.4. *In Vitro* Release Test. The controlled release experiments were performed by the dialysis bag method in phosphate buffer solutions (PB pH 7.4 and 6.4) as release medium at 37 °C and gentle stirring of 100 rpm (Heidolph MR Plug & Play Hei-Tec magnetic stirrer). Fifty milligrams of the sample was suspended in 3 mL of the buffer and then loaded in the dialysis bag (MW cutoff 14,000 Da, Sigma

https://doi.org/10.1021/acsomega.3c02288
ACS Omega 2023, 8, 26102−26121

Aldrich), which was then sank in 200 mL of the release medium. One milliliter of the liquid sample was taken off at regular intervals of time and analyzed by the Rayleigh UV1800 V/VIS spectrophotometer or UV−vis spectroscopy at λ = 266 nm (Shimadzu 1900i). Each sample was replaced by 2 mL of fresh buffer solution to keep the volume of the release medium constant. For the tests focused on the influence of the mass/volume ratio on the drug release, the experiments were performed under the same conditions, except for the amount of solid in the dialysis bag, which was 25, 50, and 75 mg. For the assessment of the ionic strength, tests in (i) PBS (phosphate-buffered saline) with different cation chloride salts found in blood (Na^+ = 134 mM, K^+ = 3.3 mM, Ca^{2+} = 1 mM, Mg^{2+} = 0.46 mM), (ii) PB (phosphate buffer), and (iii) water as release media were performed The other parameters were constant as for the tests above. The ionic strength of the release medium was calculated with eq 1:[15]

$$I = \frac{1}{2}\sum c_i z_i^2, \quad (1)$$

where I = the ionic strength, c_i = the molar concentration of each individual ion, and z_i = the charge of each ion.

The unknown concentration of drug was calculated using a calibration curve drawn for each pH and medium of release as well as each spectrophotometer. Each release test was performed in duplicate or triplicate. The measurements for the first tests at both pH values were performed on the Rayleigh UV1800 V/VIS spectrophotometer, whereas for the duplicates and triplicates, they were obtained on the Shimadzu 1900i. Therefore, the values provided in Figure 8A,B are an average of the values measured on the two different spectrophotometers. The data displayed on Figures 8C, 11, and 12 are obtained on Shimadzu only.

3. RESULTS AND DISCUSSIONS

3.1. Physicochemical Properties. *3.1.1. X-ray Diffraction Analysis.* The crystalline phases and structures of bare and 5-FU-LDH samples obtained under various aging conditions (temperature and time) were analyzed by XRD. The obtained powder X-ray diffraction patterns are illustrated in Figure 1A.

A typical XRD pattern of an LDH material consists of several characteristic peaks and can be divided into three main regions with the following typical reflections:[16−18]

> Region 1: basal 00l reflections at low Bragg angles (<30°)−interlayer content;
>
> Region 2: nonbasal 01l and/or 10l at midrange Bragg angles (30−55°)−polytypes and stacking faults;
>
> Region 3: nonbasal 11l at high Bragg angles (>60°)−intralayer content.

Each of them provides useful information about the composition and size of the interlayer gallery, layer stacking (polytypes), stacking faults, and degree of crystallinity, as briefly described below.[18−26] The presence of basal reflections is an indication of the layered arrangement of the material, and their analysis offers details on the (i) nature of the interlayer composition; (ii) nature of the magnitude of layer charge; (iii) nature of the site or location of layer charge; and (iv), to some extent, nature of intralayer composition. Quantitatively, the examination of these peaks allows the calculation of the basal spacing (d_{00l}), which consists of one brucite-like layer and one interlayer and depends on the anion size and its orientation (c parameter). The nonbasal peaks, particularly (110) reflection, is usually invariant in relation to its position at around 60°. The analysis of this reflection gives the distance between two neighboring metal cations in the layer, which corresponds to the a_0 lattice parameter. Yet, the value of this parameter suffers changes depending on the cations due to the specific ionic radius, being thus an indication of the incorporation of a certain cation in the brucite-like sheets. The mid-region of the 2θ range is particularly important because it can be explored to observe the purity of the polytype (rhombohedral (Rs) or hexagonal (Hs)); faults of layer stacking, the most common type of disorder; interstratification (intergrowth of two or more polymorphs); and turbostraticity (random orientation of successive layers along the c stacking direction).

In line with the above discussion, it can be stated that XRD patterns collected for the LDHs discussed herein (Figure 1A) are typical for the hydrotalcite-like compounds, with a basal reflection and associated harmonic at low angles 2θ and reflections at higher angles.[27,28] The corresponding diffraction peaks of each of the three 2θ regions are (003), (006), (012), (015), (018), (110), and (113).[29] Impurity peaks were not observed, indicating that the samples are of high purity and the intercalation of FU did not change their crystalline phase. According to the literature, all those peaks are indexed to a hexagonal lattice with rhombohedral R-3m symmetry.[18,29,30] However, it should be noted that the broadening and asymmetry of the (01l) peaks in the 2θ mid-range indicate the presence of stacking faults and mixed polytypes, which is a common characteristic for LDHs synthesized in the laboratory.[20,24] Apart from this observation available for all samples, it can also be noted that the aging conditions severely impacted the ordering degree of the materials, leading to materials of different crystallinities, whereas the profile of XRD patterns shows similar oriented crystal growth and stacking faults for all samples, suggesting the reproducibility of the synthesis method under similar conditions. As observed, the crystallinity of samples improves as the aging conditions become more severe. For instance, the LDH-120 sample aged hydrothermally at 120 °C for 24 h has the most intense and thinnest diffractions peaks, indicating the best-crystallized layered structure as compared with those aged at lower temperatures for a shorter time (25 and 100 °C, 16 h).[29,31] Accordingly, the peaks are sharper and more intense, particularly indicating an increase in crystallite size at higher temperature. Moreover, the stacking of slabs is more controlled, although faults, turbostratic disorders, and mixed polytypes exist, as reinforced by the shape of (01l) peaks, irrespective of the hydrothermal conditions. The appearance of the (113) reflection in the diffractogram together with the loss of the "shark's fin" shape of the (110) peak as the temperature increases plus the improved shape of (01l) peaks points to a slightly improved ordering in stacking of slabs due to the controlled conditions during crystal growth.[18,32]

The incorporation of 5-FU in samples under strictly controlled experimental conditions influenced the X-ray diffraction patterns of layered MgAl LDH. First, as shown in Figure 1A, all peaks of 5-FU containing LDHs are less intense and broader as compared with those of the homologous bare LDHs. These suggest that the presence of 5-FU did not affect the layer structure of LDHs, but it moderately reduced the crystallinity of the LDH phase.[33] It is obvious that the interactions between 5-FU and inorganic components decreased the crystallinity, whereas the general structural organization and turbostraticity were more accentuated in the

https://doi.org/10.1021/acsomega.3c02288
ACS Omega 2023, 8, 26102−26121

Table 1. Structural, Textural, and Same Characteristic Properties of the Samples[a]

	AAS	UV−vis		XRD							N2 physisorption		DLS[b]	
samples	Mg/Al mol/mol	LC %	EE %	c nm	a nm	$D_{(110)}$ nm	$D_{(003)}$ nm	$d_{(003)}$ nm	FWHM$_{(003)}$ o	t_{interl} nm	S_{BET} $m^2.g^{-1}$	V_p $cm^3.g^{-1}$	Z-average (PDI) nm	ζ mV
LDH-25	2.24			2.325	0.304	10.51	8.21	0.775	1.08	0.295	27	0.159	416 (0.35)	55.76
LDH-100	1.82			2.294	0.304	17.31	15.67	0.765	0.52	0.285	48	0.116	320 (0.23)	38.06
LDH-120	1.93			2.314	0.305	22.14	20.18	0.771	0.44	0.291	50	0.178	373 (0.31)	59.92
5-FU-LDH-25	2.09	8.34	82.39	2.342	0.304	11.37	7.42	0.781	1.22	0.301	7	0.029	469 (0.18)	40.19
5-FU-LDH-100	2.56	4.90	59.44	2.325	0.304	14.40	11.36	0.775	0.78	0.295	0	0	188 (0.25)	48.28
5-FU-LDH-120	2.28	2.63	49.76	2.312	0.304	18.74	13.10	0.771	0.68	0.291	46	0.190	221 (0.22)	57.78

[a] $a = 2d110$; $c = 3d003$; $D(110)$ = crystallite size in the a direction; $D(003)$ = crystallite size in the c direction; $d003 = \lambda/2\sin\theta$; $t$interl = $d003$ − 0.48 (brucite thickness); SBET = total specific surface area calculated with the BET equation; and Vt = total pore volume at p/po ∼0.975. [b] In water−ethanol (9/1).

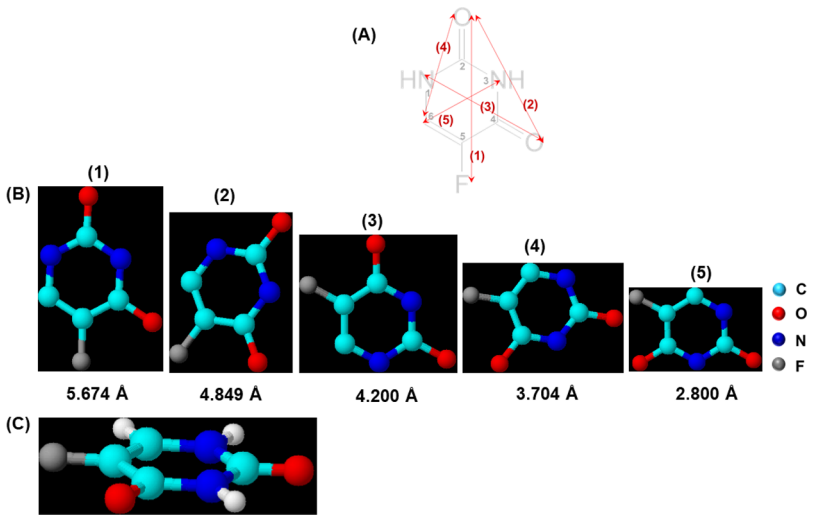

Figure 2. (A) Interatomic distances in the 5-FU molecule; (B) possible vertical positions of the FU molecule; and (C) flat position of 5-FU (from the ACD/3D software: C, 1.54; N, 1.50; O, 1.40; F, 1.35; Wiki: C, 0.70; N, 0.65; O, 0.6; F, 0.50 A).

presence of 5-FU, as shown by the higher degree of overlapping of (110) and (113) peaks in the diffractograms of the materials obtained at 25 and 100 °C. Even so, it should be mentioned that the structural quality of the synthesized organic−inorganic hybrids is superior to that of 5-FU-MgAl hybrids reported previously in the literature by other groups. Second, the shift of the (003) peak toward lower 2θ values, at least for the 5-FU-LDH-25 and 5-FU-LDH-100 samples, alongside the broadening of the peak clearly demonstrates the accommodation of the drug between the layer inside the gallery and correlates well with the decreased crystallinity (Figure 1B).[34] For the sample prepared at 120 °C, no change in the position of the (003) reflection was noted. This finding can be related either with the lowest amount of 5-FU detected in the sample (*vide infra*) or with a parallel position related to the brucite-like sheets as previously reported for certain antibiotics loaded in ZnAl-LDH.[35]

The quantitative analysis of the diffraction peaks provided the values of the microstructural parameters, that is, basal spacing (d_{003}), unit cell parameters (a and c), interlayer spacing (t_{interl}), as well as the crystallite size along a (D_{110}) and c (D_{003}) directions (Table 1).

The basal spacing, d_{003}, for the bare LDH samples has values of 0.775, 0.765, and 0.771 for LDH-25, LDH-100, and LDH-120, respectively. It is known that this parameter and implicitly the c parameter of the unit cell ($c = 3d_{003}$) strongly depend on the layer charge density and composition of the gallery-water molecules and the nature of the interlayer anion.[18,36,37] The values obtained for our samples correspond to an LDH phase with Cl^- as compensating anion.[38] For the 5-FU-LDH samples, the basal spacing slightly increased for the samples aged at 25 and 100 °C, but it was kept constant for the sample aged under more severe conditions. The corresponding values are 0.781, 0.775, and 0.771 for 5-FU-LDH-25, 5-FU-LDH-100, and 5-FU-LDH-120, respectively. The interlayer space was calculated by subtracting the thickness of the brucite-like sheet (0.48 nm)[37] from the d_{003} spacing for every sample. It is obvious that for the first two samples, the basal spacing width of the first peak enlarged, proving the replacement of Cl^- by 5-FU. To see if the incorporation of FU is supported by the molecular size and how it is oriented inside the interlayer gallery, we calculated the interatomic distances in the 5-FU molecule by using the ACD/3D software. The main distances are illustrated in Figure 2A, whereas the possible vertical positions of 5-FU are displayed in Figure 2B. As noticed, five different positions of 5-FU can be considered in the gallery of MgAl LDH. Yet, according to the values of the interlayer thickness, only one could be realistic, that is, the position in which 5-FU interacts with Al^{3+} cations in the brucite-like sheets through both O atoms simultaneously. For this case, the

https://doi.org/10.1021/acsomega.3c02288
ACS Omega 2023, 8, 26102−26121

Table 2. Correlation between the Vibration Bands of 5-FU, Shifting, and Their Intensity in the FTIR Spectra Depending on the Conditions of HT

Original wavenumber, cm^{-1}	Δ	Bond involved	Band intensity		
			25 °C	100 °C	120 °C
1657	+5	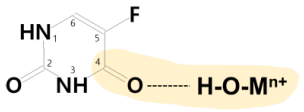	+++	++	+
1551 1541	-171 -116	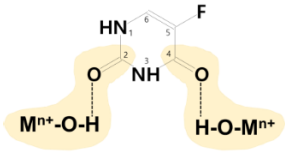			
1496	-23	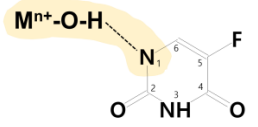			
1426	-37	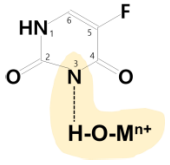			
1246	-19	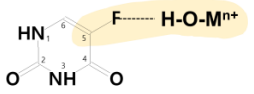			

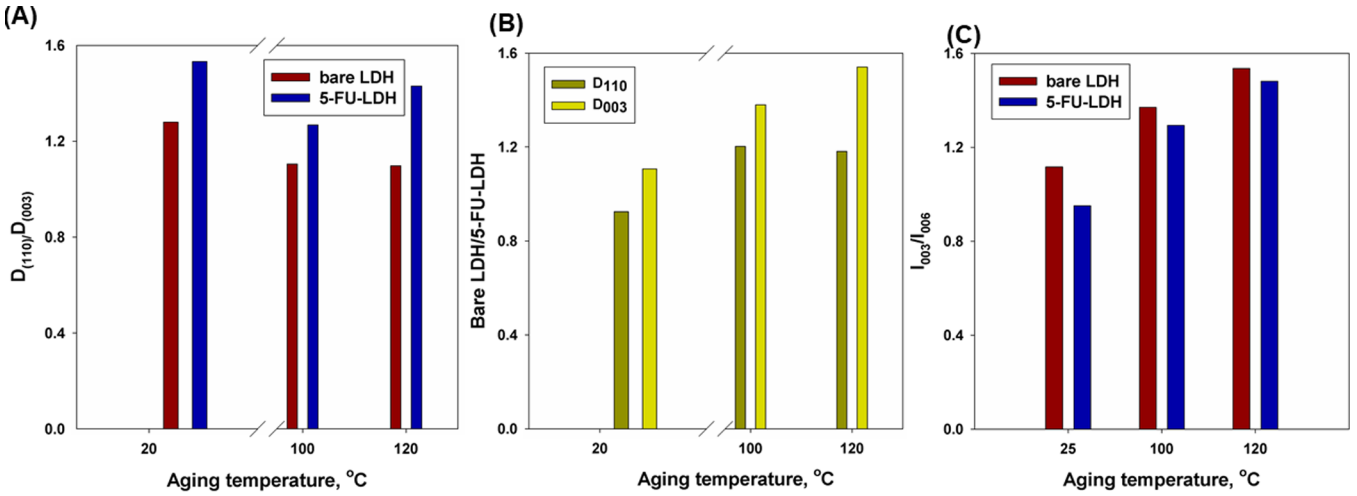

Figure 3. Analysis of the intensity ratio of main diffraction peaks for all samples. (A) $D_{(110)}/D_{(003)}$ crystallite size ratio *vs* aging temperature; (B) bare LDH/5-FU-LDH ratio for the same diffraction peak ((003) or (110)) *vs* aging temperature; and (C) I_{003}/I_{006} intensity ratio *vs* aging temperature.

space occupied by 5-FU would be ∼2.800 Å, the values of N_3...C_6 distance. In this case, it is expected that the hydrogen bonding between oxygen atoms and layers will increase. However, a horizontal orientation of the 5-FU between layers is not excluded as well (Figure 2C). For the last sample, 5-FU-LDH-120, the interlayer space is identical with that of the bare sample. Therefore, the orientation of the 5-FU molecule parallel to the positively charged octahedral inorganic sheets is more probable, and thus, a denser packing of sheets is reasonably agreed. In addition, as for the 5-FU-free samples,

https://doi.org/10.1021/acsomega.3c02288
ACS Omega 2023, 8, 26102−26121

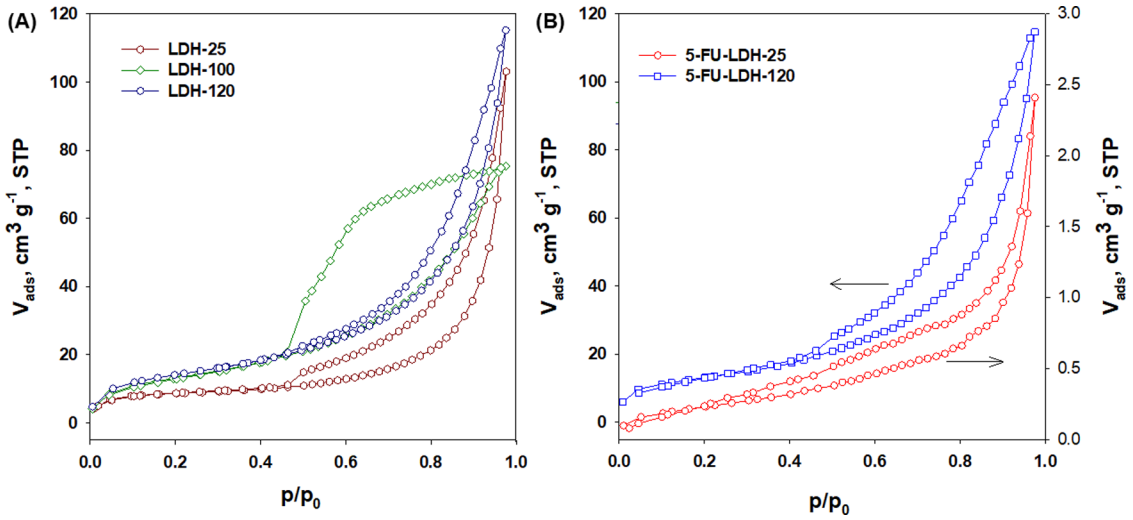

Figure 4. N_2 adsorption−desorption isotherms for LDH and 5-FU-LDH samples aged at different hydrothermal treatments (25 and 100 °C, 16 h; 120 °C, 24 h) after co-precipitation. (A) Bare LDH samples and (B) drug modified LDH samples.

the order degree in the octahedral layers increases with temperature and time because the diffraction peaks become sharper, whereas the (110) and (113) reflections are well separated. In light of the above discussed results, it can be affirmed that a random orientation of 5-FU in the synthesized LDH occurs, depending on the aging conditions. The parameter a ($a = 2d_{110}$), which corresponds to the metal−metal distance in the inorganic layer, was insensitive to the hydrothermal treatment. This result is in line with the constant composition of inorganic layers consisting of the same cations, Mg^{2+} and Al^{3+}, but it also means that the microstructure of the brucite sheets did not change.[39]

The crystallite size of all LDHs synthesized herein was calculated based on the FWHM of (003) and (110) reflections and applying the Scherrer equation. The obtained values are listed in Table 2. It was previously shown that the analysis of crystallite size on the [003] and [110] crystallographic directions may give a measure of orientation effects.[40] The crystallite size can be estimated at a glance based on the value of FWHM, which is a direct indication of the change in this parameter; the lower the FWHM is, the larger are the crystallites.[24] The size of the final crystallite can be fine-tuned by the synthesis because it is very sensitive to the experimental conditions, particularly those during the aging step when the crystal growth occurs in line with the Ostwald mechanism.[41,42] The values in Table 1 and Figure 3A,B, displaying the dependence of the crystallite size in a and c directions versus the aging temperature and LDH composition, show an obvious preference of the crystal growth on the a direction. This is supported by the values of the D_{110}/D_{003} ratio, which are above unity. Interestingly, as the temperature increases, this effect is less obvious for purely inorganic LDH (Figure 3A). This trend is generally preserved for the sample containing 5-FU, but the growth along the [110] direction was promoted when the hydrothermal treatment was performed at 120 °C for 24 h. Yet, the crystal size along the [110] direction is lower than that at 25 °C, suggesting structural constraints, maybe due to a stronger interaction between 5-FU and inorganic layers, which forces the crystal to grow in the 2D plan. If we compare the crystal size on the two directions, [110] and [113], in the absence and presence of 5-FU (Figure 3B), it can be noticed that at room temperature, the crystal growth along the (110) plane was quite similar for the two types of samples, that is, without and with 5-FU, because the size ratio is almost 1. Moreover, the crystal size of the samples aged at 25 °C is similar irrespective the composition. The change in size depending on composition, particularly, the presence of 5-FU, is more evident at higher temperatures. Therefore, the increase in temperature to 100 °C promoted the 2D growth of the layer because the crystal size along the (110) plane is 17.31 and 14.40 nm for LDH-100 and 5-FU-LDH-100, respectively, whereas that along the (003) plane is 15.67 and 11.36 nm, respectively. However, it appears that these values are optimal because the additional increase in temperature did not expand the layer in the presence of 5-FU. At this temperature, the crystal also grew but preserved the same ratio of ∼1.2 for D_{110}/D_{003} (Figure 3A). On the other hand, the presence of 5-FU caused a contraction of the crystals along the c direction because the size ratio of the crystals for LDH and 5-FU-LDH (bare LDH/5-FU-LDH) is directed toward the free FU sample (Figure 3B, D_{003}). Furthermore, this effect is more evident at higher temperatures and cannot be associated with the amount of water because both samples were synthesized under the same carefully controlled conditions. Hence, it can be hypothesized that during synthesis, the FU occupies a flat position between the layers in which it is attached. This effect can be summed up to the stacking disorder (*vide supra*) and thus explains the observed structural and crystallographic effects. On the other hand, the change in the composition of the interlayer spacing and thus the incorporation of the desired molecule can be also evaluated based on the intensity ratio of the (003) and (006) basal reflections. According to previous reports, an increase in intensity of the (006) reflection is attributed to an increase in the electron density at the midpoint of the interlayer galleries in the LDH due to the presence of a higher electron density.[28,43,44] As illustrated in Figure 3C, the intensity ratios of (003) and (006) reflections for the 5-FU-containing LDH are lower than those of the homologous inorganic LDH, indicating the replacement of chloride ions by 5-FU with higher electron density. Moreover, it can be noted that the increase in temperature decreases the electron density (the I_{003}/I_{006} for LDH and 5-FU LDH approaches each other), suggesting a lower amount of FU incorporated at higher temperatures, which correlates very well with the values of LC

https://doi.org/10.1021/acsomega.3c02288
ACS Omega 2023, 8, 26102−26121

and EE (Table 1). Indeed, the values calculated for LC, that is, 8.34, 4.90, and 2.63% for 5-FU-LDH-25, 5-FU-LDH-100, and 5-FU-LDH-120, respectively, clearly show the decrease in the amount of 5-FU incorporated between the brucite-like sheets as the HT conditions change. To note, the highest temperature of the HT was selected based on the TG curve of FU, which shows a thermal decomposition of the drug at ∼317 °C (data not shown). Regarding the composition in terms of cations, it can be observed that the Mg/Al ratio is more homogeneous for the samples containing FU instead of those purely inorganic, proving the positive impact of FU on the incorporation of the cations in line with the theoretical molar ratio (Mg/Al = 2) (Table 1).

3.1.2. N_2 Physisorption. The arrangement of plate-like crystals in an LDH material generates pores whose properties can be measured by the adsorption of pure nitrogen at −196 °C. It is obvious that, in the case of LDH, the porosity does not originate in the interlayer space but in the voids generated by a tighter or looser arrangement of the platelets because the kinetic diameter of N_2 (0.364 nm)[45] does not allow access in the interlayer space. This affirmation is however available for LDH containing commonly used inorganic anions (CO_3^{2-}, NO_3^-, Cl^-, etc.) or small organic molecules that do not enlarge the gallery enough to accommodate the N_2 molecule. The textural properties of the samples discussed herein were evaluated by adsorbing pure nitrogen on their surface free of impurities after degassing at room temperature for 16 h. Figure 4 shows the N_2 adsorption/desorption isotherms for LDHs synthetized at different hydrothermal treatments (25 and 100 °C for 16 h, 120 °C for 24 h) with and without FU.

Because the porosity measured by the isotherms is directly related to the arrangements of plate-like crystals during aging, different shapes for the isotherms and hysteresis loops can be obtained for such materials.[29,46−50] According to IUPAC classification, a *type IV isotherm* associated with the adsorption and desorption of N_2 in and from mesopores or a *type IIb isotherm* has been reported for LDH materials so far. Depending on the available space between the plate-like crystals, a hysteresis loop, usually type H3 or even a mixture of H3 and H4, due to condensation−evaporation phenomena of N_2 in slit-shaped pores and macropores can be seen in the isotherms. As seen in Figure 4, the isotherms obtained for our samples are of type IV but with different shapes of the hysteresis loop depending on the geometry of the pores and pore size distribution. The condensation−evaporation of N_2 in pores generated H3 hysteresis loops for LDH-25, LDH-120, 5-FU-LDH-25, and 5-FU-LDH-120 samples. What is intriguing is the fact that the hydrothermal treatment at 100 °C generated materials with completely opposite textural properties. Hence, for the purely inorganic sample (LDH-100), the hysteresis is type H2b, indicating the pore blocking,[51] whereas for the homologous samples containing FU, no adsorption was recorded, suggesting an organization of the crystallites in a compact architecture lacking porosity. Applying the BET equation in the range of relative pressure of 0.09−0.32, the values of the specific surface areas were calculated, and the results are listed in Table 1. The aging conditions clearly influenced the textural properties, increasing in aging temperature and time and resulting in an improved surface area. Combining these results with the improved crystallinity of samples (Figure 1) as the temperature increased, it can be assumed that the statistical arrangements of crystal during aging generated pores large enough to accommodate the N_2 molecule. Thus, the sample aged at 25 °C (LDH-25) displays a surface area of 27 $m^2\ g^{-1}$, whereas the sample aged at 120 °C for 24 h (LDH-120) has a surface area of 50 $m^2\ g^{-1}$, which is practically double the surface area. This finding underlined the positive impact of hydrothermal conditions on the formation of a more accessible porosity through the arrangement of crystals. On the other hand, the sample aged at the intermediary temperature of 100 °C displays a surface area very similar to that of the LDH-120 sample. The obtained results show that the textural properties can be tailored through the synthesis conditions for the same synthesis method. Yet, it is not necessary that results follow the same trend even for samples with similar composition of the inorganic layer. For instance, MgAl LDH (molar ratio of cation = 2:1 and Cl^- as counter anion) prepared at 90 °C by CP at high supersaturation and aged for different periods of time (2, 4, 8, and 12 h) led to samples with various surface areas between 72 and 103 $m^2\ g^{-1}$.[50] The authors correlated these values with the size of crystallites and found that the surface area is inversely proportional with the crystallite size. Indeed, it is generally assumed that the surface area decreases as the crystallinity increases.[52] In our case, this correlation is not valid because the crystallite size and surface area increased proportionally (Table 1). In ref 46, a series of MgAl LDHs with NO_3^- as counter anion were prepared by co-precipitation followed by no treatment, conventional hydrothermal treatment at 150 °C, and microwave hydrothermal treatment at 150 °C.[52] Interestingly, for the samples prepared with no thermal treatment, the surface area increased with crystallinity, whereas for those subjected to microwave hydrothermal treatment for different periods of time, the surface area decreased with the increase in crystallite size. It is obvious from the results discussed herein (ours and those reported in the literature) that the analysis of results obtained for different sets of samples can be influenced by a certain amount of subjectivism and deviations from a general rule can be obtained, as experiments always show. In certain particular cases, the size of plate-like crystals decreased the surface area of MgAl LDH samples, but in other cases, the effect was quite the opposite. Therefore, crystallite size itself cannot be considered as a robust parameter in explaining the surface area but rather in combination with their spatial organization during aging and thus the available porosity. Yet, the case of the direct proportionality between the crystal size and surface area was explained by the Ostwald ripening, which leads to larger crystallites. It was assumed that at lower aging times, the small particles blocked the pores of the growing crystals, which is not the case for mature crystals formed after a longer time of aging.[52] For the second case, when the surface area and crystallinity are inversely correlated, no satisfactory explanation was provided, but the idea of considering only the crystallite size when explaining the surface area is reinforced when discussing bulk solids made of a statistical arrangement of crystals. For the samples containing 5-FU, the same general trend was observed for materials consisting of larger crystallites for which a larger surface area was obtained. As already mentioned above, there is an exception to this rule, with the sample prepared at 100 °C (5-FU-LDH-100) displaying no porosity, most probably as a result of complete pore obstruction or very large macropores that do not fall within the range of the N_2 adsorption.[53]

3.1.3. Morphology. The morphology of the LDH and FU-LDH samples hydrothermally treated at different temperatures was determined by SEM, and the corresponding images are

https://doi.org/10.1021/acsomega.3c02288
ACS Omega 2023, 8, 26102−26121

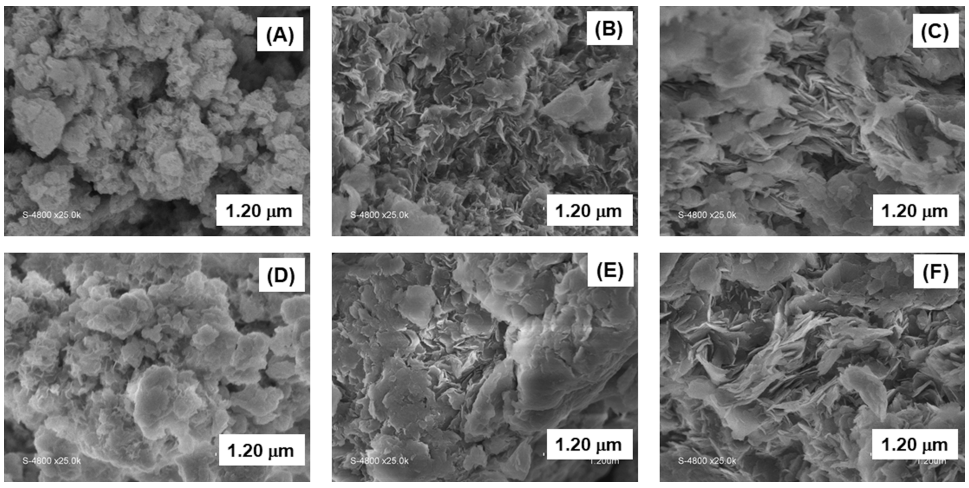

Figure 5. SEM images of the samples: (A) LDH-25, (B) LDH-100, (C) LDH-120, (D) 5-FU-LDH-25, (E) 5-FU-LDH-100, and (F) 5-FU-LDH-120.

shown in Figure 5. As can be seen, platelet-shaped particles with various degrees of crystallinity and agglomeration were obtained by increasing the temperature and time during the aging step. As discussed above for results provided by XRD and N_2 physisorption, the synthesis conditions promoted the gradual crystallization and spatial arrangement of lamellar structured crystals/particles, which are also in line with previously reported results.[31,50] Therefore, the aging under mild conditions (25 °C for 16 h) led to small layered crystals, which are organized in quite large agglomerates of particles. However, the particles can be easily discriminated against each other. As the aging temperature and time increase, the plate-like shape morphology is even better shaped, and the crystals are larger. It appears that at larger sizes, the spatial arrangement of the crystals generates more voids, which correlates well with the results of N_2 physisorption. The platelets are thin and slightly curved, especially for the sample aged at 100 °C, suggesting the existence of some constraints during crystal growth. It is worth mentioning that no apparent differences between the morphologies of LDH with and without 5-FU under the same set of aging conditions can be observed, which is a clear indication of the reproducibility of experimental conditions. Therefore, the other differences noted in the microstructure and texture of inorganic and organic−inorganic hybrid samples are directly correlated with the chemical composition and crystal growth from the appearance of the first nuclei of crystallization in the slurry at constant conditions.

3.1.4. DLS. Because the LDH samples synthesized herein are aimed at studies on cell cultures, the hydrodynamic diameter and zeta potential were also evaluated. The particle size distribution, which was obtained using the dynamic light scattering (DLS) technique, is shown as the *Z*-average in Table 1. Because of high attraction forces between particles with the formation of aggregates, as shown by SEM, the use of a solvent able to decrease the attractive forces between particles and make stable dispersions was mandatory for DLS measurements. Considering the biomedical applications of the samples, the dispersant medium has to be carefully selected to fulfill the requirements of biocompatibility. Therefore, the preparation of a stable suspension of nanoparticles for nanomedicine is very challenging because the final nanofluid has to be both stable and biocompatible. For our samples, we first tried to disperse the bare samples (without any additional chemical modification of surface) in water (1 mg mL^{-1}) followed by sonication. However, the approach was not enough to countervail the strong interactions between particles, and thus, it was not possible to prevent their almost instantaneous agglomeration and sedimentation immediately after the sonication treatment was disrupted. Moreover, it was noticed that only a part of the solid was dispersed, with a part of it lying on the bottom of the flask even during the sonication step. To improve the dispersion degree and stability of suspension, we decided to add ethanol in water and to decrease the concentration of suspension. Ethanol has the role of "prewetting". Because of its lower surface tension (s = 0.02 N m^{-1}) than water (s = 0.07 N m^{-1}), ethanol has the capacity of improving the dispersion. As a result, the prewetted particles are easier to disperse than in water.[54] Hence, a mixture of ethanol/water of 1:9 (v/v) and sonication for 30 min prior analysis were used to disperse LDH with and without 5-FU (0.7 mg mL^{-1}). Generally, the values of the *Z*-average (Table 1) for bare LDHs synthesized at different hydrothermal treatments were found to be higher as compared with the homologous samples with 5-FU. This indicates the formation of smaller agglomerates more homogeneous in size when the FU is present in the sample. On the other hand, it is well acknowledged that the size measured by DLS is overestimated because the diameter of particles reflects the size of agglomerates when the disaggregation did not result in the individual separation of particles. Therefore, when the size provided by DLS is larger than that provided by other techniques, particularly XRD and electronic microscopy, it is proof of the existence of agglomerates that are either mono- or polydispersed. This last property is measured by the polydispersity index (PDI). PDI $\leq$ 0.1 indicates highly monodispersed samples, and values of 0.1−0.4 and >0.4 are associated with moderately and highly polydispersed, respectively, samples.[55] According to the values of the *Z*-average and PDI provided in Table 1, the suspensions prepared for the LDH discussed in this work consist of aggregates with size between 221 and 469 nm that are moderately polydispersed. Interestingly, the samples containing the drug, particularly those aged at 100 and 120 °C, are made of much smaller aggregates, as compared with the inorganic counterparts, which could be attributed to an improved prewetting with ethanol in the presence of an organic molecule. On the other hand, the

https://doi.org/10.1021/acsomega.3c02288
ACS Omega 2023, 8, 26102−26121

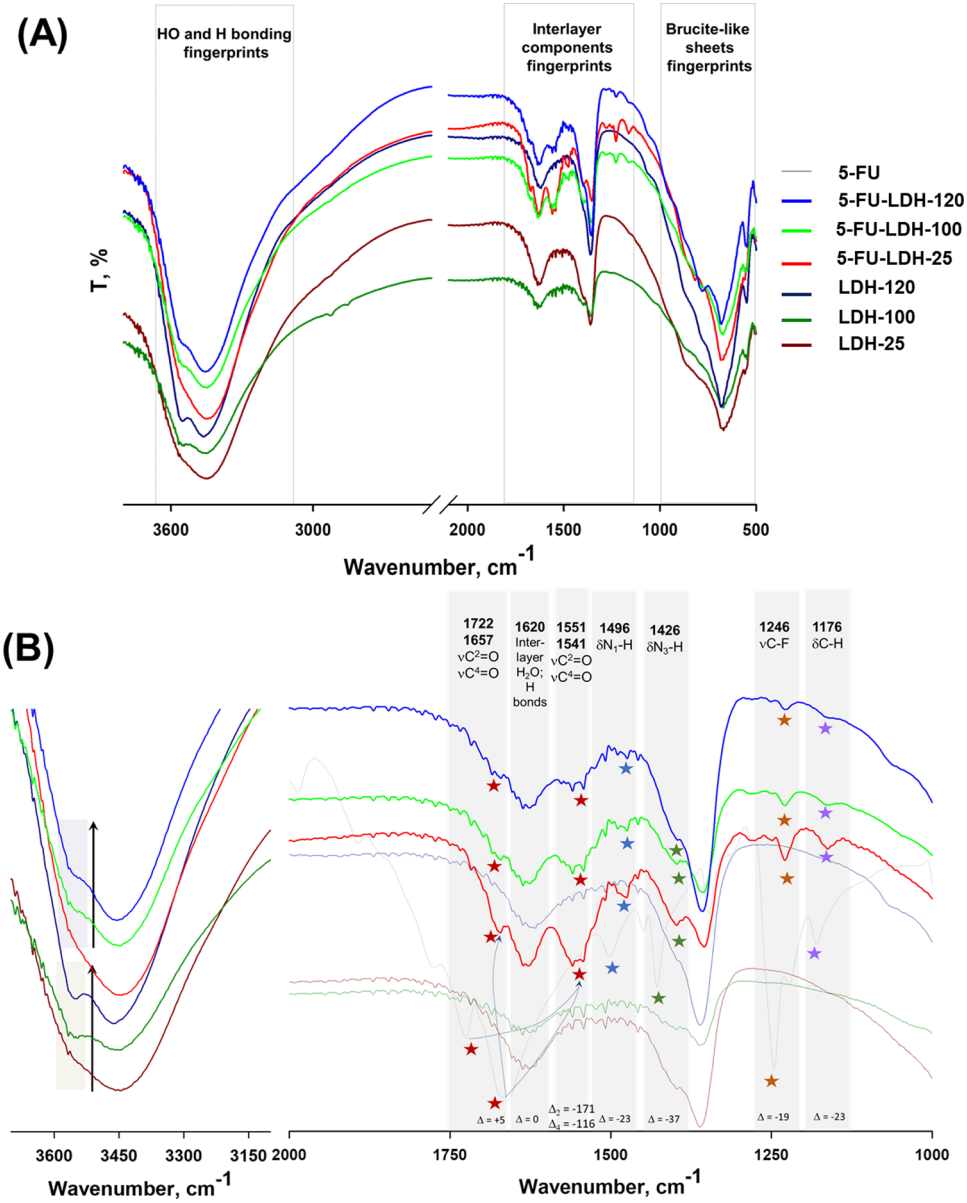

Figure 6. (A) FTIR spectra of samples. (B) Magnified image of the hydroxyl and water region (left) and interlayer ions region (right).

decrease in hydrodynamic size is in line with the decrease in crystallite size for FU-containing samples, as discussed above, an effect that could be due to an inhibition effect of anionic FU over the layer growth.[56] For the 5-FU-LDH-25, the *Z*-average is slightly higher as compared with the inorganic homologous LDH. On the other hand, these two samples have the highest values of Zeta-average in the two series. On the basis of SEM images showing a denser organization of crystals for these two samples, it is assumed that the dispersion of particles was more difficult. Still, the suspension obtained for 5-FU-LDH-25 is made of aggregates more homogeneous in size (PDI = 0.18), which is much lower than that of LDH-25 (PDI = 0.35). It is noteworthy that the results obtained for our samples correlate well with those previously reported for similar materials.[33,56−61]

On the other hand, zeta potential, which reflects the surface charge of the particles, is in the range of +38.06 and +59.92 mV. Zeta potential is a measure of the electric potential at the boundary of the double layer. In an aqueous suspension, the positively charged brucite-like layers attract negatively charged ions, which generate a thin layer on the surface. This film forms an electric double layer structure in the intimate vicinity of the LDH surface.

These values are consistent with the theory of facilitated cell internalization due to the high attraction between the positively charged nanoparticles and negatively charged phospholipids of membrane.[58] As for the XRD, the inorganic sample prepared at 100 °C (LDH-100) goes out of trend because it has a smaller zeta potential (∼38 mV) than the other two samples, that is, LDH-25 and LDH-120, for which the surface charges are of ∼56 and ∼57 mV, respectively.

3.1.5. FTIR Analysis. FTIR spectra of FU medicine, bare LDHs aged at different temperatures, and their FU-containing counterparts are illustrated in Figure 6.

All spectra show the main bands of an LDH, whereas the FU-loaded samples display additional bands typical for vibration bonds in FU.

https://doi.org/10.1021/acsomega.3c02288
ACS Omega 2023, 8, 26102−26121

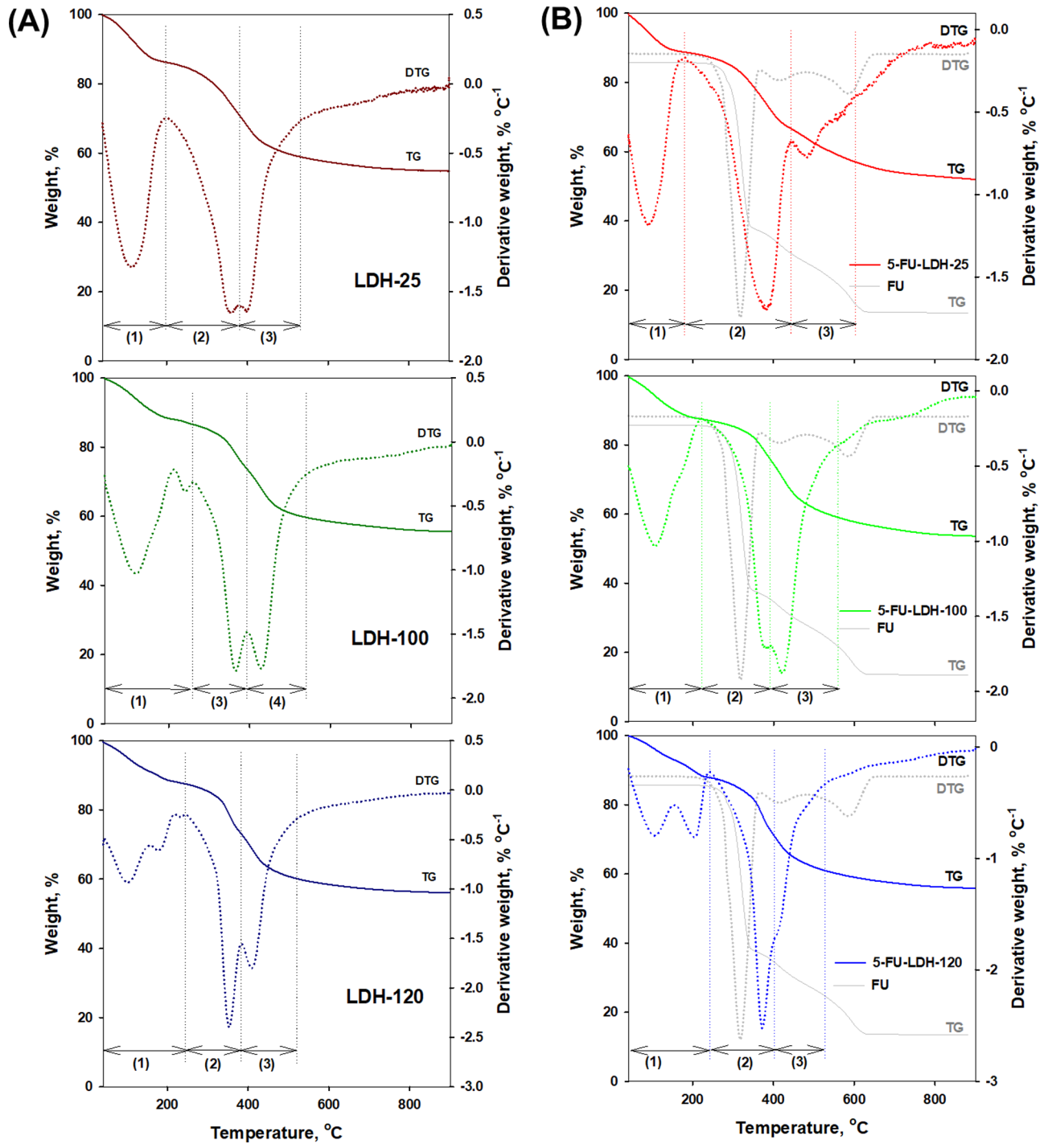

Figure 7. TG and DTG curves of (A) LDH and (B) 5-FU-LDH samples aged at different hydrothermal treatments (25 and 100 °C, 16 h; 120 °C, 24 h) after co-precipitation.

The band located between 3000 and 3600 at around 3420 cm^{-1} is attributed to overlapped stretching modes of the ν(OH) groups as well as water molecules.[62] Interestingly, for the LDH samples treated at room temperature, a shoulder at ~3510 cm^{-1} can be noticed, which evolves into a small band as the aging treatment becomes more severe. This can be correlated with the XRD results showing an improved crystallinity for the samples obtained at higher temperatures. Yet, for the samples containing FU, this band is less intense when compared with that in the purely inorganic LDH, which is also in line with XRD. It is obvious that a better crystallinity with larger crystals correlates with a larger portion of HO groups available in the samples.

The region between 1750 and 1200 cm^{-1} displays diagnostic bands of interlayer content of which those belonging to FU are primarily highlighted but also those typical to water and H bonds (Figure 6). The intense band at 1630 cm^{-1} corresponds to the deformation bending of water molecules $\delta(H_2O)$ and δ(OH) due to the intermolecular water molecules.[31,32,63] According to FTIR spectra, contamination with CO_3^{2-} (band at ~1353 cm^{-1}) was not avoidable, not so much because of the CO_2 solved in the solutions of the precursors but most

https://doi.org/10.1021/acsomega.3c02288
ACS Omega 2023, 8, 26102−26121

Table 3. Weight Loss (WT) of Samples Calculated from TG Curves

sample	T_{max} (1)	ML %	T_{max} (2)	ML %	T_{max} (3)	ML %	T_{max} (4)	ML %	total %
LDH-25	106	13.55	354	14.96	393	11.81	>393	4.85	45.18
LDH-100	111 + 236	12.95	361	12.77	424	14.25	>424	4.45	44.42
LDH-120	93 + 173 + 224	12.32	362	13.57	425	13.73	>425	4.297	43.92
5-FU-LDH-25	85	11.09	374	21.82	474	7.80	>474	7.25	47.96
5-FU-LDH-100	99 + 162	12.44	375	11.60	414	16.72	>414	5.59	46.34
5-FU-LDH-120	98 + 197	11.98	370	16.84	409	9.94	>409	5.36	44.13

probably during the washing of samples. However, the peak intensity in the 5-FU-LDH samples with higher amounts of FU is apparently decreased, implying that the amount of carbonate anion in the interlayer space was lower because of the intercalation of the drug anions.[64] The presence of 5-FU in the samples and its orientation between the layers are very obvious from the spectra of 5-FU-loaded LDHs. Moreover, the intensity of the specific bands of FU, particularly those at 1246, 1496, 1626, 1657, and 1722 cm^{-1}, corresponding to C−F, δN_1−H, δN_3−H, νC^4═O, and νC^2═O, respectively, decreases as the amount of 5-FU decreases in the samples, confirming the values of LC (Table 1).[65−67] Apparently, the 5-FU molecule participates in the interaction with the brucite-like sheets through all its ionizable groups, as well as fluoride, but with different strengths. Indeed, the pH of synthesis (∼10) favors the full ionization of 5-FU, which is thus able to be involved in bonds with all its groups, implying a stabilization of the molecule inside the host. To describe the fate of 5-FU inside LDH, Table 2 summarizes the wavenumbers for 5-FU in the original state, the shifting in the immobilized state, the group involved in the interaction, as well as the intensity of the band depending on the aging treatment.

As seen, except for the band of νC^2═O, which is positively shifted by 5 cm^{-1}, the other bands are negatively shifted to lower wavenumbers, proving the reduction of the electron density on oxygen due to the involvement in interactions with the LDH layers, most probably H bonding interactions. If for most bands the shift is moderate and their identification in the spectra of 5-FU-LDH samples is straightforward, the interpretation of the bands at 1551 and 1541 cm^{-1} is quite challenging. However, considering the ketone groups in the 5-FU molecule and their ability to get involved in H-bonding, their simultaneous involvement in H-bonding with the OH groups attached to the core cations in the brucite-like sheets is not only impossible, but apparently, it is the favored position of the molecule in the interlayer space. Therefore, the two bands at 1551 and 1541 cm^{-1} are attributed to the νC^2═O and νC^4═O, respectively, involved in the H-bonding. Such a synchronized interactions force the orientation of 5-FU in a perpendicular position inside the interlayer through the model (5) displayed in Figure 2B, at least for the samples aged at 25 and 100 °C. Indeed, for these two samples, the interlayer space calculated by XRD is very close to the size of the molecule in this position, whereas the amount of carbonate suggested by FTIR is lower. For the sample aged at 120 °C, the orientation of the molecule in such a position is not excluded but less probable. Moreover, the contribution of carbonate is the highest for this one. This orientation in addition to the interlayer thicknesses suggests that only one molecule of 5-FU is placed inside the gallery at the same place, which excludes the formation of clusters or agglomerates of 5-FU. Therefore, it is hypothesized that the 5-FU forms a single layer inside the gallery space. The band at 1176 cm^{-1} belongs to the bending vibration of the C−H bond in the pyrimidine ring of FU.[68,69] In the spectrum of 5-FU, this band is red shifted by 23 cm^{-1}, implying the interaction of the drug with the LDH through this bond, too.

The adsorption bands <1000 cm^{-1} characterize the valence vibrations between oxygen and the metal ν(M-O), and the deformation vibrations of oxygen−metal−oxygen leave ν(M-O-M).[31,70]

3.1.6. Thermogravimetry Analysis. Thermogravimetric and differential thermogravimetric (TG and DTG, respectively) behaviors of 5-FU, bare LDHs, and intercalated FU-LDHs are shown in Figure 7.

According to the literature, the thermal decomposition of LDHs is spread over three main stages that are (i) the loss of weakly physisorbed water, mostly on the external surface but also the interlayer water; (ii) the decomposition of structural hydroxyl groups; and (iii) the decomposition of the interlayer anions.[29,62,71,72] Usually, the water is desorbed up to ∼200−250 °C, whereas the dehydroxylation and decomposition of interlayer anions take place between ∼200−250 and 500 °C. These two last processes occur simultaneously, although the dehydroxylation slightly precedes and ends before the decomposition of anions. Therefore, the corresponding endothermic peaks in the DTG curves are overlapped most of the time, which make it difficult to determine a clear distinction between them. Above ∼500 °C, the formation of the amorphous metastable mixed solid oxide solution ($MgAl_2O$, MgO, Al_2O_3) takes place.

For the samples investigated in this work (Figure 7), three main steps were identified in the curves of mass loss as the temperature increases up to ∼500 °C. The values of T_{max} and corresponding mass losses (MLs) for each sample are listed in Table 3.

However, the composition and the aging conditions clearly influenced the thermal behavior of the components, as discussed below.

Stage 1: The water removal from the purely inorganic LDH (LDH-25, LDH-100, LDH-120 samples) displays several behaviors. Hence, the LDH-25 sample loses water in one single step at T_{max} = 106 °C, whereas the dehydration of the two other samples occurs in two or three steps with T_{max} at 111 and 236 °C for LDH-100 and 93, 173, and 224 °C for LDH-120. The presence of several maxima of temperature indicates that water is located in different places in the architecture formed by the arrangement of crystals during synthesis and establishes interactions of various strengths with the LDH's inorganic sheets. Yet, the total mass loss for all samples falls in the range of 12.32 and 13.55% with an average of ∼13% (Table 3), indicating similar water affinity irrespective the aging conditions. The introduction of 5-FU in the synthesis medium slightly changes the amount of water released (by

https://doi.org/10.1021/acsomega.3c02288
ACS Omega 2023, 8, 26102−26121

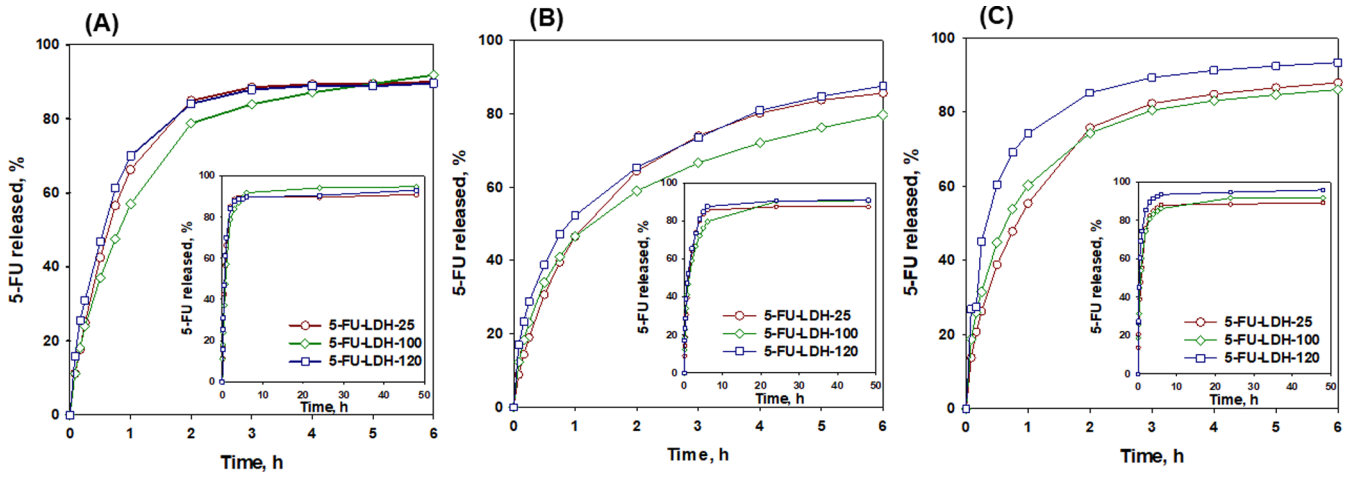

Figure 8. Release profiles of 5-FU from samples at 37 °C, 100 rpm, and different values of pH: (A) pH 7.4, (B) pH 6.4, and (C) pH 5.5 (PB).

1%), whereas the shapes of the TG curves are more or less similar to those for purely inorganic LDH samples, indicating the key role of the aging conditions in the spatial organization of crystals and entrapment of the physisorbed water.

Stage 2: The dehydroxylation and removal of Cl^- anions from the purely inorganic samples occurred in the range of ~240−530 °C. The twin peaks in the DTG curves have the T_{max} at 354/393, 361/424, and 362/425 °C for LDH-25, LDH-100, and LDH-120, respectively. As noticed, there is no significant difference between these maxima from one sample to another. What has changed is the interplay between the two peaks, especially at higher temperatures of aging. Therefore, they both become better shaped as the aging conditions become harsher. In addition, they indicate equal contributions of the species removed from the samples aged at 25 and 100 °C, but the balance is changed in favor of the first peak for the sample aged at 120 °C. In light of the literature, the first peak is attributed to the HO^- groups originating in Al-(OH)-Mg bridging units and Mg-(OH)-Mg units in that order.[71] On the other hand, the removal of chloride from LDH needs higher temperatures, usually between 400 and 900 °C.[73] However, on the basis of the distribution of the mass loss between the two peaks and the temperature at which these species are removed, it can be hypothesized that the release of hydroxyl from Mg-(OH)-Mg units partially overlaps the removal of Cl^- in the LDH-25 and LDH-100 samples. For the samples containing 5-FU, this second stage in the TG curve covers the decomposition of this organic molecule apart from the remaining inorganic charge balancing anions, which makes the interpretation of the data more challenging. In other words, it is not very evident what is the contribution of 5-FU degradation in this step for any of the samples. According to the TG curve of pure 5-FU, the decomposition takes place at 322 °C. None of the TG curves of 5-FU-LDH samples contain a peak at this temperature, clearly suggesting a shift at higher temperature in the decomposition of trapped 5-FU in LDH, pointing out the enhanced thermal stability of 5-FU due to electrostatic interactions with the brucite-like layers of LDHs. In addition, from the total mass loss in Table 3, it can be seen that the values are higher for the 5-FU-LDH samples when compared with those corresponding to 5-FU-free LDH samples, highlighting the contribution of the drug to this value. Yet, the difference is lower as the aging temperature increases, indicating the decrease in the FU amount in the sample accordingly to LC's values (Table 1).

3.2. FU Release Study. The release of the 5-FU from LDHs synthesized at different hydrothermal treatments has been investigated at 37 °C in a phosphate buffer solution at three different pH values of 7.4, 6.4, and 5.5 and with gentle stirring at 100 rpm. The release was monitored for 50 h, and the quantification of the 5-FU was achieved based on the absorbance at 266 nm. The results are shown in Figure 8A−C.

As can be seen, the general shapes of the release curves are very similar irrespective of the pH value. Yet, differences from one sample to another or from one pH value to another are obvious, especially within the first 2 h of control release. For instance, at pH 7.4, the percent of 5-FU release is 66.27, 56.95, and 69.95% for 5-FU-LDH-25, 5-FU-LDH-100, and 5-FU-LDH-120, respectively, after 1 h. After 2 h 5-of experiment, the amount of the 5-FU released increased to 78.76−84.87% for all samples. As the time increased, the amount of 5-FU identified in the release medium continued to increase, reaching almost 94.72% for the 5-FU-LDH-100 sample after 48 h. For the other two samples, the amount of 5-FU reached 90.93 and 93.04% for 5-FU-LDH-25 and 5-FU-LDH-120, respectively, at the same release time. Note that no burst release at the beginning of the experiment happened for any of the samples, highlighting the general controlled release behavior of 5-FU from a geometrically constraining environment rather than on the external surface. A similar slow release behavior together with a complete removal of 5-FU until the end of the experiment was reported for a Zn-Al LDH accommodating 5-FU-β-cyclodextrin (CMCD).[74] The slow release of 5-FU was attributed to the presence of CMCD that prolonged the time of release as compared with the bare LDH. On the other hand, the results obtained for our samples are fully attributed to the ability of pure LDH to accommodate and then slowly release 5-FU in the absence of any other release controller. The results illustrated in Figure 8A clearly indicate that rational control of the synthesis conditions allows tuning the release properties of the final nanomedicine. As the release pH decreased by a unit, meaning 10 times increase in H^+ concentration, the amount of drug released is lower than that discarded at the same release time for the experiments performed at pH 7.4. The percent of 5-FU release is 46.55, 46.61, and 52.28% for 5-FU-LDH-25, 5-FU-LDH-100, and 5-FU-LDH-120, respectively, after 1 h. The percent was higher after 2 h of release, that is, 64.55, 64.36, and

https://doi.org/10.1021/acsomega.3c02288
ACS Omega 2023, 8, 26102−26121

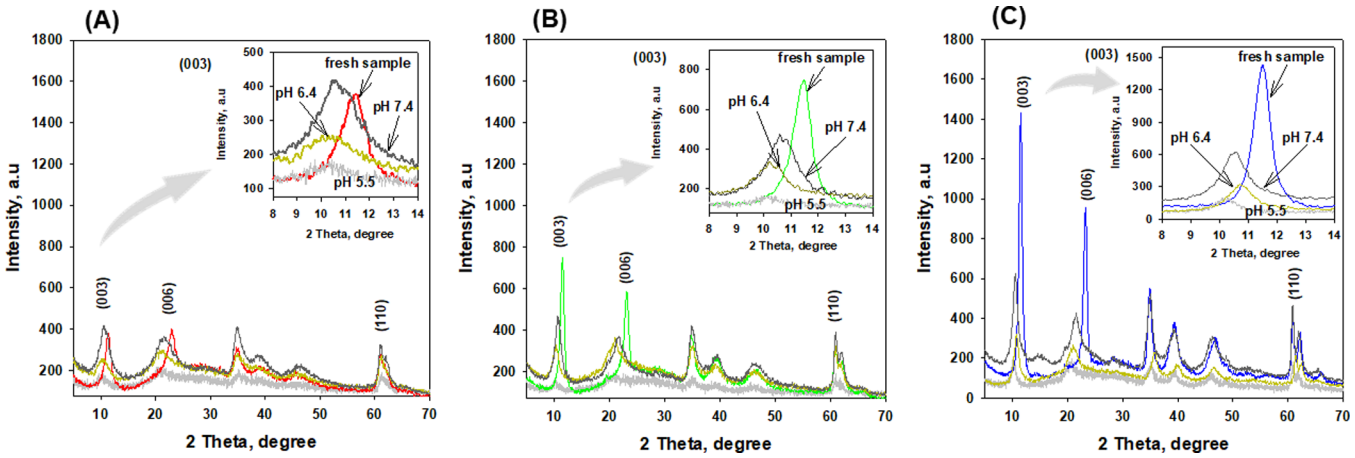

Figure 9. XRD patterns of samples before and after release of 5-FU at pH 7.4, 6.4, and 5.5: (A) 5-FU-LDH-25, (B) 5-FU-LDH-100, and (C) 5-FU-LDH-120.

65.37% for 5-FU-LDH-25, 5-FU-LDH-100, and 5-FU-LDH-120, respectively. Also, no burst release was noticed for the samples, a similar behavior as for the release at physiological pH. Further increase in acidity to pH 5.5 caused a slight increase in the amount of the released drug after the first hour of test for 5-FU-LDH-100 and 5-FU-LDH-120 samples as compared with the experiment performed at the physiological pH and a more significant increase as compared to the values obtained after release at pH 6.4 for all three samples. Thereby, the percent of FU released under these conditions is 55.32, 60.20, and 74.24% for 5-FU-LDH-25, 5-FU-LDH-100, and 5-FU-LDH-120, respectively. When the time was extended to 2 h, the amount of 5-FU released was higher, reaching the values of 75.73, 74.29, and 65.37% for 5-FU-LDH-25, 5-FU-LDH-100, and 5-FU-LDH-120, respectively. It is obvious that, in general, the release of 5-FU from LDH is sensitive to the concentration of protons. However, there is no direct proportionality between the release behavior and the pH, the amount of drug released at pH 5.5 being higher than that at pH 6.4, whereas that released at pH 6.4 is lower than that released at pH 7.4.

Most of the results published so far on the release behavior of 5-FU from MgAl-LDH showed a higher released amount at lower pH, which was mainly attributed to the partial structural loss of the solid at slightly acidic pH. However, there are studies pointing out a reverse behavior, an effect related to the lower solubility of 5-FU in a slightly acidic medium and/or formation of a complex between the 5-FU and the released cations, depending on the chemical composition of the nanocarrier. Indeed, the spectra obtained for the same amount of 5-FU recorded at pH 7.4 and 6.4 clearly show a lower absorbance of FU at pH 6.4, which can be attributed to the decreased solubility of the drug under these conditions (Figure S1). Therefore, discharging a higher amount of 5-FU from the LDH at lower pH is not excluded, but the quantified amount is not in line with this hypothesis, as explained above. On the other hand, 5-FU has several tautomeric and anionic forms whose predominance is strongly pH dependent.[75,76] Because 5-FU has several areas able to lose a proton, the mechanisms of deprotonation are very controversial and impact the release behavior, making the interpretation of data challenging. Considering this, an overestimation of the released amount at physiological pH is not excluded either. This brings us to the conclusion that a quantification of 5-FU through UV−vis spectroscopy is not enough to evaluate the amount of 5-FU released at a certain pH as appropriately as possible.

To shed more light on the release behavior from the LDHs depending on the pH and correlate this with the structural changes of the inorganic scaffold at different pH values, samples recovered after the tests were subjected to XRD and FTIR analyses. To highlight the changes in the diffractograms, the X-ray patterns for the fresh sample and after release at pH 7.4, 6.4, and 5.5 for each of the three samples (5-FU-LDH-25, 5-FU-LDH-100, and 5-FU-LDH-120) were considered and are depicted in Figure 9. Because the peak corresponding to the (003) plane plays a key role in the evaluation of the interlayer composition, magnifications of the (003) peaks for each diffractogram and sample were made and inserted in the figure.

As a general observation, it can be noticed that XRD patterns recorded for the samples sunk in the release media at the three pH values are similar to those of the fresh samples, although for the samples subjected to a more acidic pH (5.5), the changes are more obvious. Hence, all the basal and nonbasal reflections are displayed by the diffractograms in Figure 9 with the mention that the pH 5.5 considerably decreased the intensity of the diffraction peaks. Yet, the peaks are much less intense and broader as compared with those for the fresh samples irrespective of the pH, clearly indicating a much lower crystallinity and thus the occurrence of structural changes and loss of crystallinity during release experiments. As argued below, these changes are related to the value of pH, which did or did not cause the dissolution of the inorganic layers. For the samples preserved in phosphate buffer at pH 7.4, the diffractograms of all three samples show that the (003) and (006) peaks are slightly shifted at lower 2θ when compared with the fresh samples. In addition, a closer look indicated the presence of two overlapped diffraction peaks, an indication of the co-existence of two phases due to the intercalation of two anions with different sizes in the interlayer space. This phenomenon, which is more obvious for the 5-FU-LDH-25 sample (Figure 9A), is consistent with previous results.[27,77] For the nonbasal peaks, no changes in the position were noticed. For the samples investigated at pH 6.4, (003) and (006) peaks are slightly shifted at lower 2θ as compared with the original samples, but unlike those at pH 7.4, they are much less intense. Additional increase in the acidity had a significant influence on the structural organization of the samples and also on the composition of the interlayer, clearly

https://doi.org/10.1021/acsomega.3c02288
ACS Omega 2023, 8, 26102−26121

Table 4. Properties of the 5-FU-LDH Samples after Release of 5-FU at pH 7.4, 6.4, and 5.5

	AAS	XRD					
samples	Mg/Al mol/mol	c nm	a nm	$D_{(110)}$ nm	$D_{(003)}$ nm	$d_{(003)}$[a] nm	t_{interl} nm
	pH 7.4						
5-FU-LDH-25	1.84	2.488	0.304	12.93	4.08	0.829	0.349
5-FU-LDH-100	2.09	2.490	0.304	16.48	6.69	0.830	0.350
5-FU-LDH-120	2.31	2.522	0.305	22.06	8.48	0.841	0.361
	pH 6.4						
5-FU-LDH-25	1.61	2.572	0.302	6.87	3.73	0.857	0.377
5-FU-LDH-100	2.02	2.590	0.304	18.29	6.76	0.863	0.383
5-FU-LDH-120	1.67	2.468	0.302	19.09	8.85	0.823	0.343
	pH 5.5						
5-FU-LDH-25	n.d.	2.546	0.299	6.304	4.652	0.849	0.369
5-FU-LDH-100	n.d.	2.470	0.300	10.154	4.882	0.823	0.343
5-FU-LDH-120	n.d.	2.593	0.300	13.039	7.834	0.864	0.384

[a]Calculated only for the peak corresponding to the PO_4^{2-} anion.

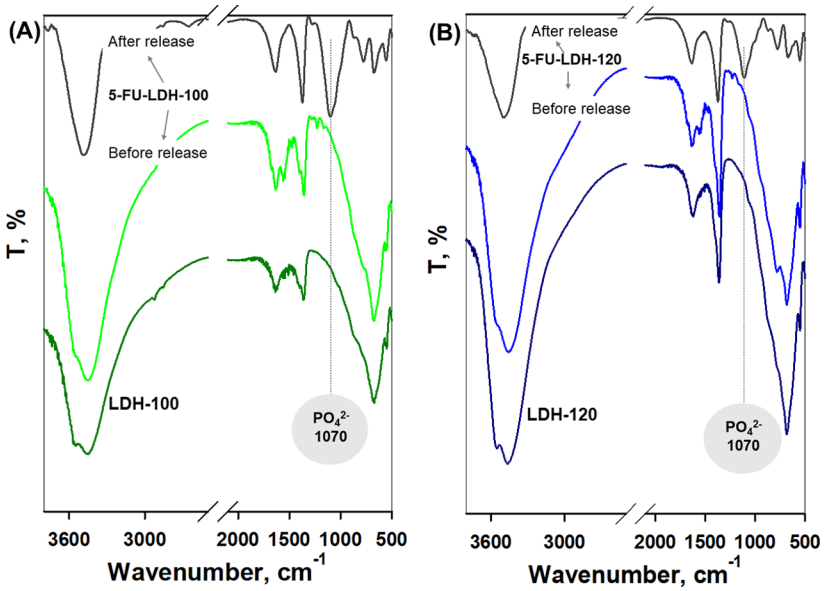

Figure 10. FTIR spectra of samples recovered after controlled release at pH 7.4: (A) 5-FU-LDH-100 and (B) 5-FU-LDH-120.

indicating the loss of the most part of the structural organization during the controlled release tests. The quantitative interpretation of the diffractograms led to the values listed in Table 4. As noticed, the values of the interlayer space for the samples tested at pH 7.4, 6.4, and 5.5 are higher than those for the fresh samples (Table 1).

On the other hand, the quantification of the Mg and Al cations in the recovered solids showed a decrease unlike the fresh samples, clearly indicating the initiation of the degradation of the nanocarriers, a phenomenon more obvious at pH 6.4 and 5.5. By combining the results provided by XRD and chemical analysis, it can be stated that the removal of 5-FU from the interlayer space is mainly due to the anion exchange between 5-FU and PO_4^{2-} in the buffer at pH 7.4. As the concentration of H^+ increases in the release medium, the dissolution of the inorganic component becomes more obvious, which led to a more noticeable change in the XRD patterns as well. Obviously, the ion exchange also takes place, as indicated by the values of the interlayer space (Table 4). These experimental results support the release of a (slightly) increased amount of 5-FU at pH 6.4, but the solubility seems to be a limiting factor for an accurate quantification (*vide supra*). In the case of pH 5.5, the dissolution of the matrix is obviously the main mechanism by which the drug is released from the carrier and at a higher rate than that of pH 6.4. Yet, the amount released at this pH is not higher than that discharged at pH 7.4, reinforcing the idea that the decreased solubility of the drug impacts the release behavior.

It should be mentioned that the results obtained herein are valuable not only for controlled drug release but for other medical applications as well. For instance, for patients with end-stage renal failure manifesting hyperphosphatemia, LDH can be used as effective adsorbers of phosphate excess, thus rebalancing the physiological concentration of this anion.[78] To confirm the nature of the anion that caused the shift of the XRD peak at lower 2θ, we performed FTIR for the samples after controlled release. Figure 10 illustrates the representative FTIR spectra for the 5-FU-LDH-100 and 5-FU-LDH-120 samples before and after release as well as those of the corresponding bare LDH for comparison purposes.

As observed, both spectra of the samples that were in contact with the phosphate buffer display a strong band at

https://doi.org/10.1021/acsomega.3c02288
ACS Omega 2023, 8, 26102−26121

1070 cm^{-1}, which is attributed to the ν_3 vibration of the PO_4^{2-} anion.[79,80] Meanwhile, the bands of FU (Figure 6) are no longer observed in the spectra in Figure 10. Yet, considering the release profile showing an incomplete release of 5-FU, this result is not necessarily due to the absence of 5-FU but to the extremely low concentration of the drug in the solid. However, considering the high affinity of divalent anions, particularly phosphate, to brucite-like sheets, it is obvious that the release of 5-FU was controlled by this phenomenon.[81] Moreover, when combined with the change in acidity, the effect was doubled by the partial dissolution of the inorganic component, which resulted in a higher amount of 5-FU released.

Because the drug release from the nanocarrier is controlled by the environment that the nanodrug reaches, it is of high importance to simulate other conditions that might play a role in this process. Moreover, the right selection of the experimental conditions is essential for the *in vitro*–*in vivo* correlation and ultimately for clinical applications. Therefore, apart from the pH, the mass/volume ratio and cations normally found in blood (ionic strength) have been investigated herein as well.

3.2.1. Influence of the Mass/Volume Ratio. The ratio between the amount of the nanodrug and the volume of the release medium is a parameter by which the amount of the released drug can be controlled. The release curves obtained for different amounts of solid (25, 50, and 75 mg) at a constant volume of suspension (3 mL) are displayed in Figure 11. The experiments were performed in PB of pH 7.4 at 37 °C and 100 rpm.

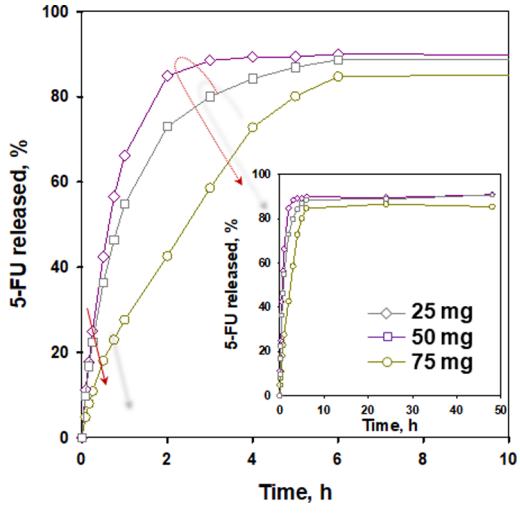

Figure 11. Release profiles of 5-FU from FU-LDH-15 samples at 37 °C, 100 rpm, PB pH 7.4, and different mass/volume ratios.

As a first general observation, it can be noticed that the amount of drug released is much lower at higher mass of solid/volume ratios within the first 6 h of the test; after that, the curves start approaching each other, indicating the release of similar concentrations of drug at longer times irrespective of the amount of solid in the release medium. For the experiments performed with 25 and 50 mg of solid, the release rates are identical in the first hour of experiment, showing no influence of this parameter on the payload discharge. As the time of release prolongs, a difference between the amount of drug discharged from the LDH depending on the starting amount of solid in the test can be observed. In the case of the test performed with 75 mg of solid nanodrug in the suspension, the slower release could be attributed to diffusional and geometric limitations associated with a higher quantity of solid. However, overall, the total drug release is not significantly influenced by the solid to liquid phase ratio. On the other hand, it should be noted that a higher amount of nanodrug implies a higher concentration of drug. In this case, it should be verified if the plasma concentration of the drug is preserved in the therapeutic range to avoid intensification of the usually occurring side effects or generation of new ones.

3.2.2. Influence of the Ionic Strengths in the Release Medium. The ionic strength of the biological environment in which the drug is released is one of the critical parameters affecting both the release behavior and the targeting property. Therefore, a change in the ionic strength can decide the fate of the loaded drug in a nanocarrier once it reaches the biological environment because it influences the nanocarrier–drug and nanocarrier–protein electrostatic interactions.[82] The ionic strength is related to the concentration of ions in the medium. When the nanodrug is administered by the parenteral way, the cations found in the blood stream could act as stimuli for drug release from the nanocarrier.[83] According to the literature, the main cations in the blood are Na^+, K^+, Ca^{2+}, and Mg^{2+} at concentrations of 134–143, 3.3–4.8, 1–1.26, and 0.46–0.66 mM, respectively.[84] Therefore, to adjust the simulated conditions of the biological environment, tests in the absence and presence of cations in the release medium were also performed. Tests in distilled water were also done for comparison purposes. The rationale was to observe any influences of the ionic strength on the release behavior of 5-FU from LDH. The release curves are displayed in Figure 12.

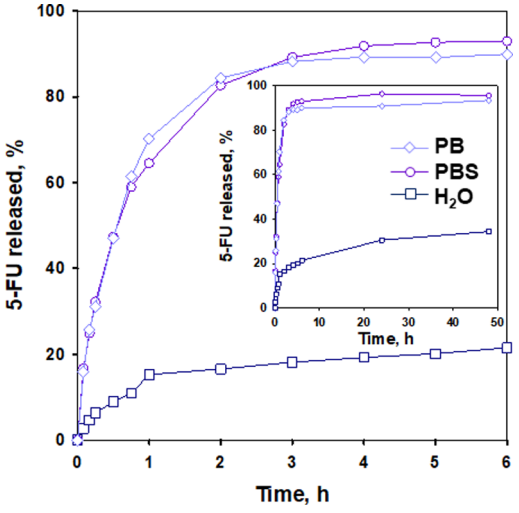

Figure 12. Release profiles of 5-FU from 5-FU-LDH-120 sample at 37 °C, 100 rpm, pH 7.4, and different release media (PB, phosphate buffer; PBS, phosphate buffer saline (Na^+, Mg^{2+}, Ca^{2+}, K^+)).

The ionic strength, *I*, of the PB and PSB calculated with eq 1, is 0.018 and 0.16 M, respectively. As noticed, the presence of cations did not influence the controlled release of drug at either the beginning of the release or total drug release. It is obvious that such nanocarriers are not affected by this parameter and the controlled release of the 5-FU from LDH with Mg and Al in the brucite-like sheets is ionic strength insensitive. On the other hand, the 5-FU release in pure water in the absence of anions from the buffer and cations is

https://doi.org/10.1021/acsomega.3c02288
ACS Omega 2023, 8, 26102–26121

considerably low. It is obvious that the ionic strength plays a critical role in the release of the drug from the nanocarrier. Considering the results reported so far in the literature, the ionic strength depends on the chemical nature of the nanocarrier. For instance, the release profiles of soluble metoprolol succinates from the water-insoluble ethyl cellulose/water-soluble hydroxypropyl cellulose-coated pellets were investigated at different ionic strengths (water, HCl solution, and phosphate and acetate buffers).[85] Apart from the other influences, such as pH and osmolality, the authors observed an increase in drug release as the ionic strength increases. Yet, the percent of drug released in water was lower than that released in the acetate buffer but higher as compared to that released in the phosphate buffer. On the contrary, other studies reported that a high ionic strength can diminish the drug release from certain matrix formulations because the amount of water available for transportation is low as a result of the decreased solubility of the hydroxypropyl methylcellulose polymer.[86,87] To the best of our knowledge, no similar study has been reported so far for inorganic carriers. However, the results displayed in Figure 12 clearly show a considerable effect of the ionic strength on the amount of the drug released, which apparently sped up the release phenomenon. This output is explained by the solubility of 5-FU, which in pure water is very low, an acknowledged shortcoming of this antimetabolite drug, which is addressed by various strategies.[88−91] These findings clearly confirm the importance of ionic strengths in the sustained release of 5-FU, being an important factor in the preparation of its pharmaceutical formulations.

The results obtained for the different factors investigated herein reveal that inappropriate conditions for the steps prior to tests on cells and *in vivo* could lead to improper predictions, significantly affecting the correlation of the results obtained in various steps on the investigation pathway of nanodrugs from the chemistry lab to the *in vivo* experiments. Therefore, a deeper understanding of the behavior of the nanodrug in *in vitro* models under various simulating conditions is recommended to shed more light on a particular type of nanomaterial used as carrier for drugs, which is beneficial for the design of optimized LDH-based nanodrugs for cancer treatment.

4. CONCLUSIONS

In this work, the successful synthesis of organic−inorganic hybrid nanomaterials consisting of MgAl-LDH carrying 5-FU in the interlayer space was discussed. The in-depth characterization of samples, particularly XRD, N_2 physisorption, and SEM, showed the formation of the typical structure of LDH. In addition, the aging step following the co-precipitation of cations in the presence of the guest 5-FU molecule is essential to carefully control the properties of the final nanomaterials. Therefore, increasing the temperature from 25 to 120 °C considerably improved the short- and long-distance order and spatial organization of the plate-like crystals. However, the higher temperature was not favorable for loading degree in the drug. The presence of the 5-FU in the interlayer gallery was confirmed by XRD, FTIR, UV−vis, and TG. The controlled release of the drug successfully hosted in the interlayer gallery showed no burst phenomenon at the beginning of the test especially at pH 7.4 and 6.4, indicating the location of the drug in confined spaces rather than on the external surface. Yet, the release at pH 5.5 was faster because of the dissolution of LDH under the acidic medium. However, because of the solubility limit of 5-FU at lower pH, the real amount of the drug released over time is (slightly) underestimated. XRD and FTIR performed for the samples recovered after controlled release showed an ion exchange between the FU and PO_4^{2-} anions of the release medium for the release at physiological pH, whereas the acidic pH gradually changes the balance toward the dissolution of the inorganic component. Keeping the experimental conditions constant and increasing the mass of the solid in the dialysis bag decreased the sustained release of the drug, whereas the ionic strength led to a faster release of 5-FU as compared with the absence of this factor. Overall, it can be stated that the careful control of the experimental conditions during the aging step when the LDH crystal grows is critical to engineer morphostructural properties and loading degree of drug in LDH-based nanomaterials as realistic candidates for nanomedicine, but it still requires many efforts to promote the translation to the clinic. In addition, an in-depth investigation of the factors involved in the *in vitro* controlled release of the encapsulated drugs in LDH is a *sine qua non* condition for the design of optimized LDH-based nanodrugs for cancer treatment.

■ ASSOCIATED CONTENT

Supporting Information

The Supporting Information is available free of charge at https://pubs.acs.org/doi/10.1021/acsomega.3c02288.

UV−vis spectra of FU solutions with different pH values and a constant concentration of FU (PDF)

■ AUTHOR INFORMATION

Corresponding Author

Brindusa Dragoi − *TRANSCEND Research Center, Regional Institute of Oncology, 700483 Iasi, Romania; Faculty of Chemistry, Al. I. Cuza University, 700506 Iasi, Romania;* orcid.org/0000-0003-1743-3083;
Email: brindusa.dragoi@yahoo.com, transcendbd@iroiasi.ro

Authors

Alina Ibanescu − *TRANSCEND Research Center, Regional Institute of Oncology, 700483 Iasi, Romania; Faculty of Chemical Engineering and Environmental Protection, "Gheorghe Asachi" Technical University of Iasi, 700050 Iasi, Romania*

Dragos-Ioan Olariu − *TRANSCEND Research Center, Regional Institute of Oncology, 700483 Iasi, Romania; Faculty of Chemistry, Al. I. Cuza University, 700506 Iasi, Romania*

Doina Lutic − *TRANSCEND Research Center, Regional Institute of Oncology, 700483 Iasi, Romania; Faculty of Chemistry, Al. I. Cuza University, 700506 Iasi, Romania;* orcid.org/0000-0002-3959-0891

Vasile Hulea − *Institut Charles Gerhardt Montpellier, UMR 5253, CNRS-UM-ENSCM, Montpellier 34296, France;* orcid.org/0000-0003-2652-5174

Complete contact information is available at: https://pubs.acs.org/10.1021/acsomega.3c02288

Author Contributions

The manuscript was written through contributions of all authors. All authors have given approval to the final version of the manuscript.

https://doi.org/10.1021/acsomega.3c02288
ACS Omega 2023, 8, 26102−26121

Notes

The authors declare no competing financial interest.

■ ACKNOWLEDGMENTS

This work was supported by the following projects: WIDESPREAD-06-2020-ERA Chairs/H2020 ERA-Chair projects grant agreement no. 952390/2020; Ministry of Education and Research, CNCS/CCCDI-UEFISCDI, project number PN-III-P3-3.6-H2020-2020-0105/35/2021; COST Actions CA21111 and CA21159.

■ REFERENCES

(1) Moreau Bachelard, C.; Coquan, E.; du Rusquec, P.; Paoletti, X.; Le Tourneau, C. Risks and benefits of anticancer drugs in advanced cancer patients: A systematic review and meta-analysis. *EClinicalMedicine* **2021**, *40*, 101130−101138.

(2) *Strategic Research and Innovation Agenda For Nanomedicine, 2016−2030*; ETP Nanomedicine: 2016.

(3) Sarder, A.; Rabbani, G.; Chowdhury, A. S. M. H. K.; Sobhani, M.-E. Molecular Basis of Drug Interactions of Methotrexate, Cyclophosphamide and 5-Fluorouracil as Chemotherapeutic Agents in Cancer. *Biomed. Res. Ther.* **2015**, *2*, 196−206.

(4) Zhang, N.; Yin, Y.; Xu, S. J.; Chen, W. S. 5-Fluorouracil: mechanisms of resistance and reversal strategies. *Molecules* **2008**, *13*, 1551−1569.

(5) Ye, H.; Shen, Z.; Yu, L.; Wei, M.; Li, Y. Manipulating nanoparticle transport within blood flow through external forces: an exemplar of mechanics in nanomedicine. *Proc. R. Soc. A* **2018**, *474*, 20170845.

(6) Park, D.-H.; Choi, G.; Choy, J.-H. Bio-Layered Double Hydroxides Nanohybrids for Theranostics Applications. In *Photofunctional Layered Materials*; Springer International Publishing Switzerland: 2015; pp. 137−175, DOI: 10.1007/978-3-319-16991-0_4.

(7) Anselmo, A. C.; Modery-Pawlowski, C. L.; Menegatti, S.; Kumar, S.; Vogus, D. R.; Tian, L. L.; Chen, M.; Squires, T. M.; Sen Gupta, A.; Mitragotri, S. Platelet-like nanoparticles: mimicking shape, flexibility, and surface biology of platelets to target vascular injuries. *ACS Nano* **2014**, *8*, 11243−11253.

(8) Brown, T. D.; Habibi, N.; Wu, D.; Lahann, J.; Mitragotri, S. Effect of Nanoparticle Composition, Size, Shape, and Stiffness on Penetration Across the Blood-Brain Barrier. *ACS Biomater. Sci. Eng.* **2020**, *6*, 4916−4928.

(9) Klemkaite, K.; Prosycevas, I.; Taraskevicius, R.; Khinsky, A.; Kareiva, A. Synthesis and characterization of layered double hydroxides with different cations (Mg, Co, Ni, Al), decomposition and reformation of mixed metal oxides to layered structures. *Open Chem.* **2011**, *9*, 275−282.

(10) Delhoyo, C. Layered double hydroxides and human health: An overview. *Appl. Clay Sci.* **2007**, *36*, 103−121.

(11) Cao, Z.; Li, B.; Sun, L.; Li, L.; Xu, Z. P.; Gu, Z. 2D Layered Double Hydroxide Nanoparticles: Recent Progress toward Preclinical/Clinical Nanomedicine. *Small Methods* **2020**, *4*, 1900343.

(12) Choi, G.; Eom, S.; Vinu, A.; Choy, J.-H. 2D Nanostructured Metal Hydroxides with Gene Delivery and Theranostic Functions; *A Comprehensive Review*. *Chem. Rec.* **2018**, *18*, 1033−1053.

(13) Yan, L.; Gonca, S.; Zhu, G.; Zhang, W.; Chen, X. Layered double hydroxide nanostructures and nanocomposites for biomedical applications. *J. Mater. Chem. B* **2019**, *7*, 5583−5601.

(14) Ameena Shirin, V. K.; Sankar, R.; Johnson, A. P.; Gangadharappa, H. V.; Pramod, K. Advanced drug delivery applications of layered double hydroxide. *J. Controlled Release* **2021**, *330*, 398−426.

(15) *Contemporary Practice in Clinical Chemistry*, 4th ed.; Clarke, W.; Marzinke, M., Eds.; AACC & Academic Press: San Diego, USA, 2020; p 1035.

(16) Duan, X.; Lu, J.; Evans, D. G. Assembly Chemistry of Anion-intercalated Layered Materials. In *Modern Inorganic Synthetic Chemistry*; Elsevier: Amsterdam, The Netherlands, 2010; pp. 375−404.

(17) Thomas, G. S.; Kamath, P. V. Line broadening in the PXRD patterns of layered hydroxides: The relative effects of crystallite size and structural disorder. *J. Chem. Sci.* **2006**, *118*, 127−133.

(18) Evans, D. G.; Slade, R. C. T. Structural Aspects of Layered Double Hydroxides. In *Layered Double Hydroxides. Structure and Bonding*; Duan, X.; Evans, D.G., Ed.; Springer: Berlin, Heidelberg, 2005; Vol. *19*.

(19) Sławiński, W. A.; Sjåstad, A. O.; Fjellvåg, H. Stacking Faults and Polytypes for Layered Double Hydroxides: What Can We Learn from Simulated and Experimental X-ray Powder Diffraction Data? *Inorg. Chem.* **2016**, *55*, 12881−12889.

(20) Shivaramaiah, R.; Navrotsky, A. Energetics of order-disorder in layered magnesium aluminum double hydroxides with interlayer carbonate. *Inorg. Chem.* **2015**, *54*, 3253−3259.

(21) Ramesh, T. N.; Jayashree, R. S.; Kamath, P. V. Disorder in Layered Hydroxides: Diffax Simulation of the X-ray Powder Diffraction Patterns of Nickel Hydroxide. *Clays Clay Miner.* **2003**, *51*, 570−576.

(22) Thomas, G. S.; Rajamathi, M.; Vishnu Kamath, P. DIFFaX Simulations of Polytypism and Disorder in Hydrotalcite. *Clays Clay Miner.* **2004**, *52*, 693−699.

(23) Leont'eva, N. N.; Drozdov, V. A.; Bel'skaya, O. B.; Cherepanova, S. V. Structural Analysis of Defects in Layered Double Hydroxides and Related Mixed Oxides. *Russ. J. Gen. Chem.* **2020**, *90*, 509−522.

(24) Radha, A. V.; Shivakumara, C.; Kamath, P. V. DIFFaX simulations of stacking faults in layered double hydroxides (LDHs). *Clays Clay Miner.* **2005**, *53*, 520−527.

(25) Vaysse, C.; Guerlou-Demourgues, L.; Demourgues, A.; Lazartigues, F.; Fertier, D.; Delmas, C. New (Ni, Co)-based layered double hydroxides with intercalated oxometalate (Mo, W) species, obtained by chimie douce reactions. *J. Mater. Chem.* **2002**, *12*, 1035−1043.

(26) Leont'eva, N. N.; Cherepanova, S. V.; Stepanova, L. N.; Drozdov, V. A.; Lavrenov, A. V. Structural Aspects of "Memory Effect" for MgGa LDHs: New Data Obtained by Simulation of XRD Patterns for 1D Disordered Crystals. *Crystals* **2022**, *12*, 629.

(27) Wu, G.; Wang, L.; Yang, L.; Yang, J. Factors Affecting the Interlayer Arrangement of Transition Metal−Ethylenediaminetetraacetate Complexes Intercalated in Mg/Al Layered Double Hydroxides. *Eur. J. Inorg. Chem.* **2007**, *2007*, 799−808.

(28) Gago, S.; Pillinger, M.; Sá Ferreira, R. A.; Carlos, L. D.; Santos, T. M.; Gonçalves, I. S. Immobilization of Lanthanide Ions in a Pillared Layered Double Hydroxide. *Chem. Mater.* **2005**, *17*, 5803−5809.

(29) Silva Neto, L. D.; Anchieta, C. G.; Duarte, J. L. S.; Meili, L.; Freire, J. T. Effect of Drying on the Fabrication of MgAl Layered Double Hydroxides. *ACS Omega* **2021**, *6*, 21819−21829.

(30) Yang, K.; Yan, L.-g.; Yang, Y.-m.; Yu, S.-j.; Shan, R.-r.; Yu, H.-q.; Zhu, B.-c.; Du, B. Adsorptive removal of phosphate by Mg−Al and Zn−Al layered double hydroxides: Kinetics, isotherms and mechanisms. *Sep. Purif. Technol.* **2014**, *124*, 36−42.

(31) Iqbal, M. A.; Fedel, M. Effect of Synthesis Conditions on the Controlled Growth of MgAl−LDH Corrosion Resistance Film: Structure and Corrosion Resistance Properties. *Coatings* **2019**, *9*, 30.

(32) Mahjoubi, F. Z.; Khalidi, A.; Cherkaoui, O.; Elmoubarki, R.; Abdennouri, M.; Barka, N. Treatment of textile effluents by chloride-intercalated Zn-, Mg- and Ni-Al layered double hydroxides. *J. Water Reuse Desalin.* **2017**, *7*, 307−318.

(33) Li, L.; Gu, W.; Chen, J.; Chen, W.; Xu, Z. P. Co-delivery of siRNAs and anti-cancer drugs using layered double hydroxide nanoparticles. *Biomaterials* **2014**, *35*, 3331−3339.

(34) Gao, X.; Lei, L.; O'Hare, D.; Xie, J.; Gao, P.; Chang, T. Intercalation and controlled release properties of vitamin C intercalated layered double hydroxide. *J. Solid State Chem.* **2013**, *203*, 174−180.

https://doi.org/10.1021/acsomega.3c02288
ACS Omega 2023, 8, 26102−26121

(35) Mishra, G.; Dash, B.; Sethi, D.; Pandey, S.; Mishra, B. K. Orientation of Organic Anions in Zn-Al Layered Double Hydroxides with Enhanced Antibacterial Property. *Environ. Eng. Sci.* **2017**, *34*, 516−527.
(36) Choi, G.; Kim, T.-H.; Oh, J.-M.; Choy, J.-H. Emerging nanomaterials with advanced drug delivery functions; focused on methotrexate delivery. *Coord. Chem. Rev.* **2018**, *359*, 32−51.
(37) Cavani, F.; Trifirò, F.; Vaccari, A. Hydrotalcite-type Anionic Clays: Preparation, Properties and Applications. *Catal. Today* **1991**, *11*, 173−301.
(38) Liu, H. M.; Zhao, X. J.; Zhu, Y. Q.; Yan, H. DFT study on MgAl-layered double hydroxides with different interlayer anions: structure, anion exchange, host-guest interaction and basic sites. *Phys. Chem. Chem. Phys.* **2020**, *22*, 2521−2529.
(39) Xiao, G. F.; Zeng, H. Y.; Huang, Q. J.; Zhang, W.; Du, J. Z.; Duan, H. Z.; Chen, C. R. Facile Preparation of Modifying Layered Double Hydroxide Nanoparticles for Drug Delivery. *J. Nanosci. Nanotechnol.* **2018**, *18*, 5256−5265.
(40) Matos, C. R.; Xavier, M. J.; Barreto, L. S.; Costa, N. B., Jr.; Gimenez, I. F. Principal component analysis of X-ray diffraction patterns to yield morphological classification of brucite particles. *Anal. Chem.* **2007**, *79*, 2091−2095.
(41) Zhao, Y.; Li, F.; Zhang, R.; Evans, D. G.; Duan, X. Preparation of Layered Double-Hydroxide Nanomaterials with a Uniform Crystallite Size Using a New Method Involving Separate Nucleation and Aging Steps. *Chem. Mater.* **2002**, *14*, 4286−4291.
(42) Tathod, A. P.; Gazit, O. M. Fundamental Insights into the Nucleation and Growth of Mg−Al Layered Double Hydroxides Nanoparticles at Low Temperature. *Cryst. Growth Des.* **2016**, *16*, 6709−6713.
(43) Chang, Z. *Controllable preparation, structural characterization and application of rare earth element-containing layered double hydroxides*. Doctoral dissertation, Université Blaise Pascal, Clermont-Ferrand II, France, 2012.
(44) Beaudot, P.; De Roy, M. E.; Besse, J. P. Preparation and Characterization of Intercalation Compounds of Layered Double Hydroxides with Metallic Oxalato Complexes. *Chem. Mater.* **2004**, *16*, 935−945.
(45) Kunze, S.; Groll, R.; Besser, B.; Thöming, J. Molecular diameters of rarefied gases. *Sci. Rep.* **2022**, *12*, 2057.
(46) Benito, P.; Labajos, F. M.; Rocha, J.; Rives, V. Influence of microwave radiation on the textural properties of layered double hydroxides. *Microporous Mesoporous Mater.* **2006**, *94*, 148−158.
(47) Rives, V. *Layered Double Hydroxides: Present and Future*; Nova Science New York: 2001; p 262−264.
(48) Zhou, C.-H.; Beltramini, J. N.; Lin, C.-X.; Xu, Z.-P.; Lu, G. Q.; Tanksale, A. Selective oxidation of biorenewable glycerol with molecular oxygen over Cu-containing layered double hydroxide-based catalysts. *Catal. Sci. Technol.* **2011**, *1*, 111−122.
(49) Malherbe, F.; Forano, C.; Besse, J.-P. Use of organic media to modify the surface and porosity properties of hydrotalcite-like compounds. *Microporous Mater.* **1997**, *10*, 67−84.
(50) Guo, Y.; Cui, X.; Li, Y.; Zhang, Q.; Wang, H. The Effect of Aging Time on the Properties of Mg-Al-CO3 Layered Double Hydroxides and Its Application as a Catalyst Support for TiO2. *J. Nanosci. Nanotechnol.* **2016**, *16*, 5653−5661.
(51) Cychosz, K. A.; Thommes, M. Progress in the Physisorption Characterization of Nanoporous Gas Storage Materials. *Engineering* **2018**, *4*, 559−566.
(52) Trujillano, R.; González-García, I.; Morato, A.; Rives, V. Controlling the Synthesis Conditions for Tuning the Properties of Hydrotalcite-Like Materials at the Nano Scale. *ChemEngineering* **2018**, *2*, 3−15.
(53) Gregg, S. J.; Sing, K. S. W.; Salberg, H. W. *Adsorption, Surface Area and Porosity*, 2nd ed.; Academic Press: London, 1982.
(54) Hartmann, N. B.; Jensen, K. A.; Baun, A.; Rasmussen, K.; Rauscher, H.; Tantra, R.; Cupi, D.; Gilliland, D.; Pianella, F.; Riego Sintes, J. M. Techniques and Protocols for Dispersing Nanoparticle Powders in Aqueous Media-Is there a Rationale for Harmonization? *J. Toxicol. Environ. Health, Part B* **2015**, *18*, 299−326.
(55) Bhattacharjee, S. DLS and zeta potential - What they are and what they are not? *J. Controlled Release* **2016**, *235*, 337−351.
(56) Chen, J.; Shao, R.; Li, L.; Xu, Z. P.; Gu, W. Effective inhibition of colon cancer cell growth with MgAl-layered double hydroxide (LDH) loaded 5-FU and PI3K/mTOR dual inhibitor BEZ-235 through apoptotic pathways. *Int. J. Nanomed.* **2014**, *9*, 3403−3411.
(57) Li, L.; Gu, Z.; Gu, W. Y.; Xu, Z. P. Direct synthesis of layered double hydroxide nanosheets for efficient siRNA delivery. *RSC Adv.* **2016**, *6*, 95518−95526.
(58) Zuo, H.; Chen, W.; Cooper, H. M.; Xu, Z. P. A Facile Way of Modifying Layered Double Hydroxide Nanoparticles with Targeting Ligand-Conjugated Albumin for Enhanced Delivery to Brain Tumour Cells. *ACS Appl. Mater. Interfaces* **2017**, *9*, 20444−20453.
(59) Oh, J. M.; Choi, S. J.; Lee, G. E.; Kim, J. E.; Choy, J. H. Inorganic metal hydroxide nanoparticles for targeted cellular uptake through clathrin-mediated endocytosis. *Chem. − Asian J.* **2009**, *4*, 67−73.
(60) Chakraborty, M.; Dasgupta, S.; Soundrapandian, C.; Chakraborty, J.; Ghosh, S.; Mitra, M. K.; Basu, D. Methotrexate intercalated ZnAl-layered double hydroxide. *J. Solid State Chem.* **2011**, *184*, 2439−2445.
(61) Gu, Z.; Zuo, H.; Li, L.; Wu, A.; Xu, Z. P. Pre-coating layered double hydroxide nanoparticles with albumin to improve colloidal stability and cellular uptake. *J. Mater. Chem. B* **2015**, *3*, 3331−3339.
(62) Álvarez, M. G.; Chimentão, R. J.; Barrabés, N.; Föttinger, K.; Gispert-Guirado, F.; Kleymenov, E.; Tichit, D.; Medina, F. Structure evolution of layered double hydroxides activated by ultrasound induced reconstruction. *Appl. Clay Sci.* **2013**, *83-84*, 1−11.
(63) Mkaddem, H.; Rosales, E.; Pazos, M.; Ben Amor, H.; Sanromán, M. A.; Meijide, J. Anti-inflammatory drug diclofenac removal by a synthesized MgAl layered double hydroxide. *J. Mol. Liq.* **2022**, *359*, No. 119207.
(64) Huang, Q.-J.; Zeng, H.-Y.; Zhang, W.; Feng, B.; Liu, X.-J.; Duan, H.-Z.; Ding, P.-X. Loading kinetics of 5-fluorouracil onto hydrotalcite and in vitro drug delivery. *J. Taiwan Inst. Chem. Eng.* **2016**, *60*, 525−531.
(65) Singh, J. S. FTIR and Raman spectra and fundamental frequencies of 5-halosubstituted uracils: 5-X-uracil (X=F, Cl, Br and I). *Spectrochim. Acta, Part A* **2012**, *87*, 106−111.
(66) Socrates, G. *Infrared and Raman Characteristic Group Frequencies, Tables and Charts*, Third Edition ed.; John Wiley & Sons, LTD: West Sussex PO19 IUD, England, 2001.
(67) Ten, G. N.; Burova, T. G.; Baranov, V. I. Analysis of IR Spectra and Hydrogen Bonds of Uracil and N1,N3-Deuterouracil. *J. Struct. Chem.* **2001**, *42*, 555−563.
(68) Tamami, B.; Farjadian, F.; Ghasemi, S.; Allahyari, H. Synthesis and applications of polymeric N-heterocyclic carbene palladium complex-grafted silica as a novel recyclable nano-catalyst for Heck and Sonogashira coupling reactions. *New J. Chem.* **2013**, *37*, 2011−2018.
(69) Ezugwu, C. I.; Mousavi, B.; Asrafa, M. A.; Mehta, A.; Vardhan, H.; Verpoort, F. An N-heterocyclic carbene based MOF catalyst for Sonogashira cross-coupling reaction. *Catal. Sci. Technol.* **2016**, *6*, 2050−2054.
(70) Shabanian, M.; Hajibeygi, M.; Raeisi, A. FTIR characterization of layered double hydroxides and modified layered double hydroxides. In *Layered Double Hydroxide Polymer Nanocomposites*; Sabu Thomas, S. D., Ed.; Elsevier Science, Woodhead Publishing: 2020; pp. 77−101.
(71) Chmielarz, L.; Kuśtrowski, P.; Rafalska-Łasocha, A.; Majda, D.; Dziembaj, R. Catalytic activity of Co-Mg-Al, Cu-Mg-Al and Cu-Co-Mg-Al mixed oxides derived from hydrotalcites in SCR ofNO with ammonia. *Appl. Catal., B* **2002**, *35*, 195−210.
(72) Yang, W.; Kim, Y.; Liu, P. K. T.; Sahimi, M.; Tsotsis, T. T. A study by in situ techniques ofthe thermal evolution ofthe structure ofa Mg−Al−CO3 layered double hydroxide. *Chem. Eng. Sci.* **2002**, *57*, 2945−2953.
(73) Kloprogge, J. T.; Kristóf, J.; Frost, R. L. Thermogravimetric analysis-mass spectrometry (TGA-MS) of hydrotalcites containing

https://doi.org/10.1021/acsomega.3c02288
ACS Omega 2023, 8, 26102−26121

CO32-, NO3 -, Cl-, SO4 2- or ClO4. In *Proceedings of the 12th International Clay Conference;* Elsevier: Bahia Blanca, Argentina, 2001.
(74) Jin, L.; Liu, Q.; Sun, Z.; Ni, X.; Wei, M. Preparation of 5-Fluorouracil/β-Cyclodextrin Complex Intercalated in Layered Double Hydroxide and the Controlled Drug Release Properties. *Ind. Eng. Chem. Res.* **2010**, *49*, 11176−11181.
(75) Abdrakhimova, G. S.; Ovchinnikov, M. Y.; Lobov, A. N.; Spirikhin, L. V.; Ivanov, S. P.; Khursan, S. L. 5-Fluorouracil solutions: NMR study of acid-base equilibrium in water and DMSO. *J. Phys. Org. Chem.* **2014**, *27*, 876−883.
(76) Wielińska, J.; Nowacki, A.; Liberek, B. 5-Fluorouracil-Complete Insight into Its Neutral and Ionised Forms. *Molecules* **2019**, *24*, 3683.
(77) Carneiro, J.; Caetano, A. F.; Kuznetsova, A.; Maia, F.; Salak, A. N.; Tedim, J.; Scharnagl, N.; Zheludkevich, M. L.; Ferreira, M. G. S. Polyelectrolyte-modified layered double hydroxide nanocontainers as vehicles for combined inhibitors. *RSC Adv.* **2015**, *5*, 39916−39929.
(78) Forano, C.; Hibino, T.; Leroux, F.; Taviot-Guého, C. Layered Double Hydroxides. In *Handbook of Clay Science*; Elsevier: Amsterdam, 2006; pp. 1021−1097, DOI: 10.1016/S1572-4352(05)01039-1.
(79) Sokol, D.; Vieira, D. E. L.; Zarkov, A.; Ferreira, M. G. S.; Beganskiene, A.; Rubanik, V. V.; Shilin, A. D.; Kareiva, A.; Salak, A. N. Sonication accelerated formation of Mg-Al-phosphate layered double hydroxide via sol-gel prepared mixed metal oxides. *Sci. Rep.* **2019**, *9*, 10419.
(80) Kim, T.-H.; Lundehøj, L.; Nielsen, U. G. An investigation of the phosphate removal mechanism by MgFe layered double hydroxides. *Appl. Clay Sci.* **2020**, *189*, No. 105521.
(81) Khan, S. B.; Alamry, K.; Alyahyawi, N.; Asiri, A. Controlled release of organic-inorganic nanohybrid:cefadroxil intercalated Zn-Al-layered double hydroxide. *Int. J. Nanomed.* **2018**, *Volume 13*, 3203−3222.
(82) Yadav, K. S.; Mishra, D. K.; Deshpande, A.; Pethe, A. M., Levels of Drug Targeting. In *Basic Fundamentals of Drug Delivery*; Academic Press: 2019; pp. 269−305, DOI: 10.1016/B978-0-12-817909-3.00007-8.
(83) Rudko, M.; Urbaniak, T.; Musiał, W. Recent Developments in Ion-Sensitive Systems for Pharmaceutical Applications. *Polymer* **2021**, *13*, 1641.
(84) Zhang, W. Point Of Care Testing of Ionized Magnesium in Blood with Potentiometric Sensors - Opportunities and Challenges. *Am. J. Biomed. Sci.* **2011**, 301−312.
(85) Chen, L.; Yang, G.; Chu, X.; Gao, C.; Wang, Y.; Gong, W.; Li, Z.; Yang, Y.; Yang, M.; Gao, C. Polymer Distribution and Mechanism Conversion in Multiple Media of Phase-Separated Controlled-Release Film-Coating. *Pharmaceutics* **2019**, *11*, 80.
(86) Asare-Addo, K.; Conway, B. R.; Larhrib, H.; Levina, M.; Rajabi-Siahboomi, A. R.; Tetteh, J.; Boateng, J.; Nokhodchi, A. The effect of pH and ionic strength of dissolution media on in-vitro release of two model drugs of different solubilities from HPMC matrices. *Colloids Surf., B* **2013**, *111*, 384−391.
(87) Nashed, N.; Chan, S.; Lam, M.; Ghafourian, T.; Nokhodchi, A. Effect of pH, Ionic Strength and Agitation Rate on Dissolution Behaviour of 3D-Printed Tablets, Tablets Prepared from Ground Hot-Melt Extruded Filaments and Physical Mixtures. *Biomedicines* **2023**, *11*, 375.
(88) Arias, J. L. Novel strategies to improve the anticancer action of 5-fluorouracil by using drug delivery systems. *Molecules* **2008**, *13*, 2340−2369.
(89) Kavitha, K.; Nalini, C. N. An Investigation on Enhancement of Solubility of 5 Fluorouracil by Applying Complexation Technique-Characterization, Dissolution and Molecular-Modeling Studies. *J. Appl. Pharm. Sci.* **2013**, *3*, 162−166.
(90) Zorrilla-Veloz, R. I.; Stelzer, T.; López-Mejías, V. Measurement and Correlation of the Solubility of 5-Fluorouracil in Pure and Binary Solvents. *J. Chem. Eng. Data* **2018**, *63*, 3809−3817.
(91) Paul, R.; Paul, S. Exploration on the drug solubility enhancement in aqueous medium with the help of endo-functionalized molecular tubes: a computational approach. *Phys. Chem. Chem. Phys.* **2021**, *23*, 18999−19010.

https://doi.org/10.1021/acsomega.3c02288
ACS Omega 2023, 8, 26102−26121